THESIS FOR THE DEGREE OF DOCTOR OF PHILOSOPHY

Modelling of the Daytime and Night-time Urban Thermal Environment

Shiho Onomura

UNIVERSITY OF GOTHENBURG

FACULTY OF SCIENCE

DOCTORAL THESIS A159

UNIVERSITY OF GOTHENBURG

DEPARTMENT OF EARTH SCIENCES

GOTHENBURG, SWEDEN 2015

Shiho Onomura

Modelling of the daytime and night-time urban thermal environment

A159 2015

ISBN (Print): 978-91-628-9768-0

ISBN (PDF): 978-91-628-9769-7

ISSN: 1400-3813

Internet ID: http://hdl.handle.net/2077/41613

Printed by Ineko AB

Distribution: Department of Earth Sciences, University of Gothenburg, Sweden

ABSTRACT

The world's urban population is expected to increase over the coming decades. To maintain and improve the health and well-being of urban citizens, it is important to increase our knowledge and develop methods for evaluating the urban thermal environment to support urban planning. The aim of this thesis is to develop and improve the modelling of the urban thermal environment, particularly enabling modelling to be done using readily available data and hardware. The thesis has four parts. The first and second parts describe the development of simplified models for computing day- and night-time urban site-specific air temperatures (T_a) at street level. The third part presents an analysis of nocturnal cooling in the near-surface atmosphere and discusses its implications for modelling the night-time T_a. The final part presents improvements of the SOLWEIG model that allow it to account for different ground cover types when computing the mean radiant temperature (T_{mrt}). T_{mrt} is one of important variables governing outdoor human thermal comfort.

The daytime model was developed by coupling a convective boundary layer slab model and an urban land surface model. It is used to perturb routinely observed T_a values from a reference site (e.g. rural, airport) to obtain urban site-specific T_a data. The night-time model was developed empirically based on the concept of nocturnal cooling progressing in two distinct phases. It simulates cooling rates at a height of 2 m in urban canyons depending on building density. The modelled cooling rates are then used to estimate the night-time T_a. The models were designed to run on commodity computers and to require only standard meteorological input data and land surface information, all of which are widely available. Both models perform well in terms of temporal development and accuracy.

Nocturnal cooling in the lower layer of the near-surface atmosphere (between the ground and a height of 60-70 m) was shown to be more intense and to evolve differently over time compared to cooling in the upper layer (up to 105 m). In addition, two distinct cooling phases were detected in both layers. Around sunset, the rates of cooling diverge decreasing with increasing height in both layers. However, within a few hours after sunset, the cooling rates converge in the lower layer, while the height-dependent cooling rate differences in the upper layer remain largely unchanged over night. The persistent differences in the upper layer are linked to the formation of a stabilized atmospheric layer. The pattern and intensity of cooling depend on the synoptic weather situation (defined in terms of the Lamb weather type) and the season. These results imply that the night-time model can be applied to other heights with a few modifications.

A ground cover scheme in the SOLWEIG model was developed based on field observations conducted in Gothenburg. The effects of different ground materials (grass and asphalt) on T_{mrt} were a few degrees, i.e. about one tenth of the shadowing effect of buildings. This suggests that changing the ground cover type may not be as effective as shadowing at mitigating radiant heat loads during hot days. Nevertheless, it could contribute to a reduction in T_{mrt} when shadowing is not an option. An evaluation study showed that the model also predicted T_{mrt} reasonably well over different ground surfaces in London, UK.

The models presented in this thesis will be implemented in a climate service tool, which can be used for various scientific and practical applications.

Key words: urban thermal environment, microclimate modelling, air temperature, mean radiant temperature, nocturnal cooling rates, synoptic weather types

PREFACE

This thesis includes the following four papers:

I. **Onomura, S.**, C. S. B. Grimmond, F. Lindberg, B. Holmer, and S. Thorsson, 2015: Meteorological forcing data for urban outdoor thermal comfort models from a coupled convective boundary layer and surface energy balance scheme. *Urban Climate,* **11,** 1-23. DOI:10.1016/j.uclim.2014.11.001

II. **Onomura, S.**, F. Lindberg, B. Holmer, and S. Thorsson, 2016: Intra-urban nocturnal cooling rates: development and evaluation of the NOCRA model. *Meteorological Applications*. In press.

III. **Onomura, S.**, B. Holmer, D. Chen and S. Thorsson, 2016: Vertical distribution of nocturnal cooling rates in a suburban area on the Swedish west coast. *Manuscript*.

IV. Lindberg, F., **S. Onomura**, C. S. B. Grimmond, 2016: Influence of ground surface characteristics on the mean radiant temperature in urban areas. *International Journal of Biometeorology*. In press. DOI:10.1007/s00484-016-1135-x

The studies were conducted in collaboration with colleaqes at the following institutions: Department of Earth Sciences, University of Gothenburg; Department of Geography, King's College London, UK; Department of Meteorology, University of Reading, UK.

In Paper I, *S. Onomura* conducted the model coupling, the evaluation, the sesitivity analysis and writing, in collaboration with the co-authors.

In Paper II, *S. Onomura* had the main responsibility for the data analysis, the model development including programming, the model evaluation and writing. The model concept was developed based on a number of discussions with the co-authors.

In Paper III, *S. Onomura* was responsible for the data analysis and writing. The data of synoptic weather conditions were produced by Prof. Deliang Chen.

In Paper IV, *S. Onomura* contributed to the field measurements, the data analysis and writing.

TABLE OF CONTENTS

LIST OF ABBREVIATIONS

Abbreviation	Unit	Description
BLUEWS	-	C**BL** model + S**UEWS**
BLUMPS	-	C**BL** model + L**UMPS**
CBL	-	**C**onvective **B**oundary **L**ayer
CR_1	K h^{-1}	Initial cooling rate at the start of Phase 1 cooling
CR_2	K h^{-1}	Initial cooling rate at the start of Phase 2 cooling
CR_{peak}	K h^{-1}	Most intensive cooling rate at night
CRIF	-	**C**ooling **R**ate **I**mpact **F**actor
GIS	-	**G**eographic **I**nformation **S**ystem
ISL	-	**I**nertial **S**ub-**L**ayer
IUHI	-	**I**ntra-**U**rban **H**eat **I**sland
$K\downarrow$	W m^{-2}	Incoming short-wave radiation
$L\uparrow$	W m^{-2}	Outgoing long-wave radiation
LUMPS	-	**L**ocal scale **U**rban **M**eteorological **P**arameterization **S**cheme
LWT	-	**L**amb **W**eather **T**ype
NOCRAM	-	**NO**cturnal **C**ooling **RA**te **M**odel
P	hPa	Air pressure
Q_H	W m^{-2}	Sensible heat flux
Q_E	W m^{-2}	Latent heat flux
q	g kg^{-1}	Specific air humidity
RH	%	Relative humidity
Ri_b	-	Bulk Richardson number
RSL	-	**R**oughness **S**ub-**L**ayer
SL	-	**S**urface **L**ayer
SOLWEIG	-	**SO**lar and **L**ong **W**ave **E**nvironmental **I**rradiance **G**eometry-model
SUEWS	-	**S**urface **U**rban **E**nergy and **W**ater balance **S**cheme
SVF	-	**S**ky **V**iew **F**actor
T_a	ºC	Air temperature
T_{max}	ºC	Maximum daily air temperature
T_{mrt}	ºC	Mean radiant temperature
t	s	Time
t_1	s	Time when Phase 1 cooling starts
t_2	s	Time when Phase 2 cooling starts
t_{end}	s	Time when nocturnal cooling finishes in the morning
t_{peak}	s	Time when cooling rate is most intensive
UBL	-	**U**rban **B**oundary **L**ayer
UCL	-	**U**rban **C**anopy **L**ayer
UHI	-	**U**rban **H**eat **I**sland
ULSM	-	**U**rban **L**and **S**urface **M**odel
UMEP	-	**U**rban **M**ulti-scale **E**nvironmental **P**redictor
U	m s^{-1}	Wind speed
z_i	m	Boundary layer height
Θ	K	Potential air temperature

Part I

Synthesis

1. INTRODUCTION

Today more than half of the world's population live in urban areas, and this proportion is expected to increase to around two thirds by 2050 (United Nations 2014). Therefore, increasing numbers of people will be exposed to urban environments in the future.

The urban environment is characterized by built-up sites with higher radiant heat loads and air temperatures (T_a) than those observed at rural/open sites. This is known as the urban heat island (UHI) and intra-UHI (IUHI) effect. The radiant heat load on a human body is often expressed in terms of the mean radiant temperature (T_{mrt}), which is one of the most important meteorological variables governing the human energy balance and thermal comfort outdoors (Mayer and Höppe 1987). The relationship between daytime and night-time T_a, T_{mrt} and heat-related health risks has been described in detail (Thorsson et al. 2014). High day- and night-time T_a and T_{mrt} values are associated with increased mortality. Therefore, nocturnal cooling and relatively low night-time T_a values are important because they enable people to recuperate from daytime heat stress, especially during consecutive hot days.

The urban thermal environment is controlled by surface characteristics (i.e. the materials that comprise the surface, its morphology, and so on), by the prevailing synoptic weather conditions, and by the season. The overnight development of the UHI and IUHI effects depends on differences in cooling rates (i.e. changes in temperature per hour) between sites, which in turn depend on the sites' surface characteristics (Oke and Maxwell 1975). Nocturnal cooling is weakened within urban areas because urban land is extensively covered with buildings and impervious surfaces, which favour heat storage and heating (Oke 1987). This is partly why urban T_{mrt} values are higher than in rural areas. The local thermal environment is also strongly dependent on the local weather conditions, which are governed by the synoptic atmospheric circulation and vary with the seasons. For instance, heat waves (i.e. periods of extremely high temperatures that are sustained for several days), are associated with blocking anti-cyclones (Galarneau et al. 2012; Pfahl 2014). To protect and improve the health and well-being of urban citizens, particularly during such extreme events, it is important to accurately characterize the urban thermal environment and to make the resulting knowledge available in a format that can be utilised by urban planners and practitioners.

Due to the complexity of the urban environment, the modelling of the urban environment is challenging and tends to be complex and computationally expensive (Baklanov et al. 2009). Thus, such models are unsuitable for many practical applications.

The objective of this thesis is thus to develop and improve the modelling of the urban thermal environment, especially the prediction of T_a and T_{mrt}, enabling models to be computationally inexpensive and use only readily available input data. This overall

objective was subdivided into four smaller goals, each of which is addressed in one of the appended papers:

- To develop a model with minimal input and computational requirements for calculating representative daytime T_a in an urban area of interest, by coupling a convective boundary layer (CBL) slab model and a urban land surface model (**Paper I**).

- To develop a nocturnal cooling rate model to calculate urban site-specific T_a, based on the concept of nocturnal cooling progressing in two distinct phases, proposed by Holmer et al. (2007) (**Paper II**).

- To provide new insights into nocturnal cooling development in the near-surface atmosphere, its dependence on synoptic weather situations, and its seasonal variation (**Paper III**). Also, to suggest ways of further developing the night-time model presented in Paper II.

- To improve the modelling of T_{mrt} by taking into account the influence of different ground surface materials, and to assess the effectiveness of changing the ground cover types as a way of modifying the radiative thermal environment (**Paper IV**).

2. BACKGROUND – modelling of the urban thermal environment

2.1. The thermal environment in the urban boundary layer

Thermal conditions close to the ground respond to changes in the lower part of the troposphere, which is referred to as the urban boundary layer (UBL) when it lies over an urban land surface (Oke 1976). T_a and T_{mrt} therefore depend on the characteristics of the urban surface (e.g. its composition and morphology), the weather conditions and the diurnal day and night cycle (Stull 1988; Garratt 1992; Barlow 2014).

The daytime UBL is divided into four different sub-layers (Figure 1, left). From the ground surface, the sublayers are called the Urban Canopy Layer (UCL), the Roughness Sublayer (RSL), the Inertial Sublayer (ISL) and the Convective Boundary Layer (CBL). Together, the lowest three layers (i.e. the UCL, RSL and ISL) are known as the surface layer (SL), which corresponds roughly to the bottom 10 % of the UBL (Stull 1988). In general, the UCL is defined as the portion of the atmosphere that lies below the mean height of surface obstacles such as buildings and trees and is thus within their canopy (Oke 1976). The values of T_a and T_{mrt} in the UCL have strong and direct effects on human thermal comfort. The RSL starts at the upper limit of the canopy and extends upwards to 2–5 times the height of the UCL (Barlow 2014). The atmosphere in the UCL and RSL is spatially heterogeneous due to the influence of individual surface obstacles. Therefore, the urban thermal environment is also heterogeneous over micro-scale distances of 10^{-1}–10^{3} m. The atmosphere in the ISL is considered to be horizontally homogeneous at the local scale (i.e. over horizontal distances of 10^{2}–10^{4} m). Within this layer, the influences of individual surface elements are mixed and homogenized, making conditions here representative of local-scale effects (Grimmond and Oke 2002). In the CBL, the atmosphere is both vertically and horizontally homogeneous because of strong daytime convection driven by upward buoyancy and mechanical turbulence (Garratt 1992). Therefore, the thermal conditions within the CBL are also rather homogeneous.

In contrast, the night-time UBL is characterized by a shallow surface layer whose properties evolve throughout the night (Figure 1, right). This layer is often characterized by a thermally stratified atmosphere, called a stable layer, whose properties are controlled by long-wave radiative flux divergence. However, it is very sensitive to the local surface energy balance and regional or synoptic weather situations (Barlow 2014). Therefore, the stable layer is easily transformed by external disturbances, e.g. rural air advection and cloud appearance. Consequently, the night-time UBL can be nearly neutral. The unsteady state of the atmosphere has made it difficult to obtain a robust understanding of nocturnal cooling process in the near-surface atmosphere, especially in heterogeneous urban areas. This also makes it difficult to reliably estimate night-time T_a values for urban areas.

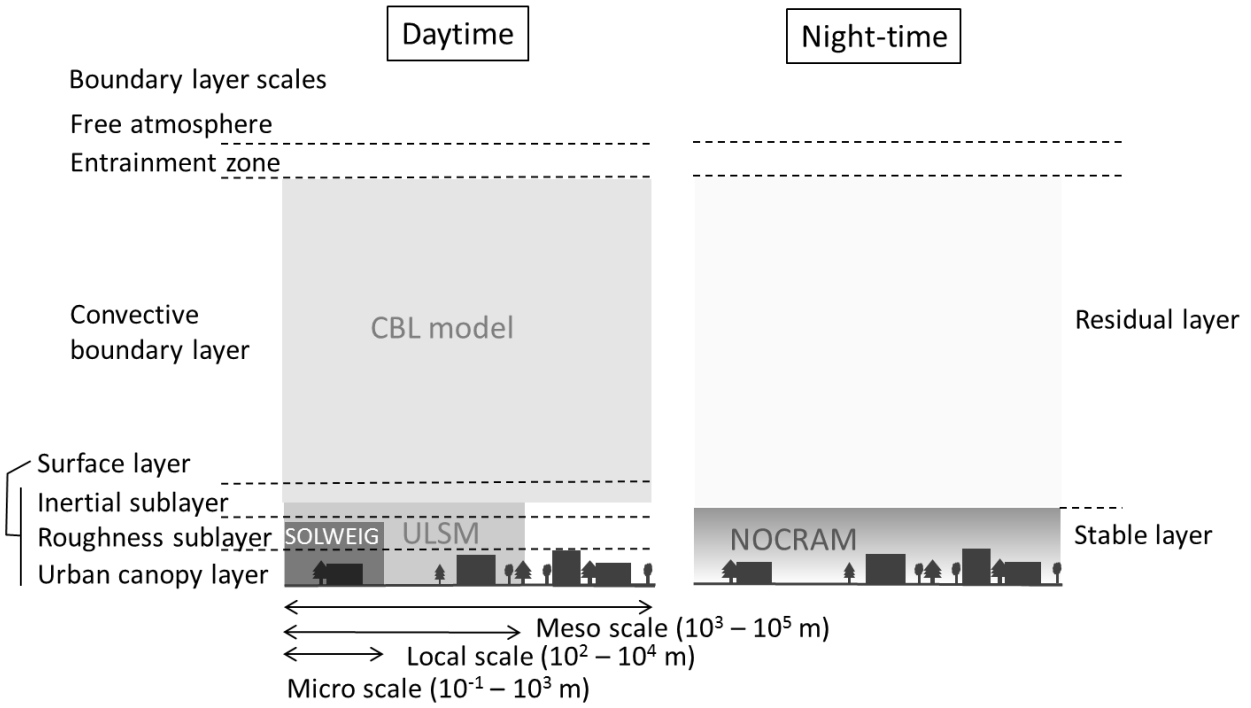

Figure 1. Daytime sublayers (left) and night-time sublayers (right) in the urban boundary layer with the corresponding scales and models used.

As mentioned above, the UHI and IUHI effects result from differences in nocturnal cooling rates between urban/densely built-up sites and rural/open sites. These differences are attributed to differences in site characteristics such as building density, surface material, the amount of vegetation, and the presence of anthropogenic heat (Oke 1987). At street level, nocturnal cooling progresses through two distinct phases (Holmer et al. 2007), which have been observed in several cities and various climate zones across the world (e.g. Oke and Maxwell 1975; Lee 1979; Johnson 1985; Upmanis et al. 1998; Runnalls and Oke 2000; Chow and Roth 2006; Holmer et al. 2013). Around sunset, the cooling rate at an urban/densely built-up site is lower than at a rural/open site, whereas during the night cooling rates at both sites converge to the same low rate, gradually decreasing until sunrise. This is why the UHI (IUHI) intensity is stabilized a few hours after sunset and remains constant through the night (Fortuniak et al. 2006). The pattern as well as the intensity of cooling vary greatly with the weather conditions and seasons (Kidder and Essenwanger 1995; Magee et al. 1999; Runnalls and Oke 2000; Holmer et al. 2007; Chow and Svoma 2011). The physical concepts of UHI/IUHI intensities and cooling rates have been established in several studies (e.g. Runnalls and Oke 2000; Acevedo and Fitzjarrald 2001; Acevedo and Fitzjarrald 2003; Holmer et al. 2007), which can be utilized for the modelling of night-time T_a.

2.2. Modelling of daytime urban site-specific air temperatures

The modelling of T_a within urban areas is very complex because of the spatial heterogeneity of urban settings. Computational fluid dynamics (CFD) models simulate the

intricate details of atmospheric motions and scalar concentrations around buildings at street level by resolving a series of thermodynamic and fluid mechanic equations. However, because of their high computational cost (Baklanov et al. 2009), such simulations are mainly conducted for scientific purposes (Ashie et al. 2005; Kanda 2006).

Alternatively, air temperatures could be modelled by coupling a meso-scale atmospheric model to an Urban Land Surface Model (ULSM) (e.g. Bohnenstengel et al. 2011; Stewart et al. 2013; Theeuwes et al. 2014) or using analytical models (Erell and Williamson 2006; Bueno et al. 2013), which have relatively modest computational requirements. In the coupling method, the meso-scale model calculates T_a using urban surface turbulent heat fluxes, while the ULSM calculates the heat fluxes using T_a. ULSMs also estimate other components (e.g. net all-wave radiation and storage heat fluxes) in the surface energy balance (SEB). However, the lowest level at which meso-scale models can calculate T_a is usually above the RSL. Some theoretical methods for estimating the T_a in the UCL based on the output of a meso-scale model have been proposed (e.g. Theeuwes 2015). In addition, the use of multi-dimensional meso-scale models has been explored as a way of overcoming this problem. For daytime simulations, the CBL slab model (also known as the box model) can be used, under the assumption that the daytime atmosphere is well-mixed and spatially homogeneous. The model is rather simple but simulates the growth and the properties of the CBL reasonably well (Raupach 2001). In contrast, analytical models calculate urban site-specific T_a values on the basis of meteorological data recorded at a reference station. They are typically paired with ULSMs to account for the impact of differences in surface heat fluxes between the urban and reference sites. The atmospheric boundary layer that forms above the urban and reference sites is treated in a relatively simple way.

2.3. Modelling of night-time urban site-specific air temperatures

As mentioned above, modelling of night-time T_a near the surface is generally problematic. Nocturnal cooling is driven by multiple heat exchange processes such as long-wave radiative flux divergence, sensible heat flux divergence and air advection (Estournel et al. 1986), each of which can be calculated in numerical models. However, the calculations are not simple because the contributions of radiative and sensible heat flux divergence to cooling rates vary as the night progresses (Schaller 1977) and also with height (André and Mahrt 1982; Sun et al. 2003; Steeneveld et al. 2010). Moreover, these heat exchanges are highly sensitive to the vertical profile of T_a and aerosol concentrations (Schaller 1977; Ha and Mahrt 2003). Therefore, the modelling of night-time T_a is more complex and costly than that of daytime T_a, and existing approaches are not satisfactory (Steeneveld et al. 2010; Steeneveld 2014). It would therefore be desirable to develop analytical or empirical methods for estimating night-time T_a. In addition, there is a need for more information on the physical process occurring in the night-time UBL.

2.4. Influence of ground cover materials on the mean radiant temperature

T_{mrt} is defined as the uniform temperature of an imaginary enclosure in which radiant heat transfer from the human body equals the radiant heat transfer in the actual non-uniform enclosure (ASHRAE 2001). It thus measures the radiant heat load from the surroundings to which a human body is exposed. Because of the complex urban settings, T_{mrt} can vary widely over short distances in urban areas. The spatial variation in daytime T_{mrt} is chiefly influenced by shadow patterns, i.e. variation in direct shortwave radiation, which are determined by the presence of obstructing objects such as trees and buildings, as well as the general topography (Lindberg and Grimmond 2011). Increasing the level of shadowing, primarily by trees and bushes, could thus be a relatively straightforward and practical way of reducing daytime heat stress and mitigating high daytime T_{mrt} values in urban areas (e.g. Andersson-Sköld et al. 2015). Another possible way of regulating the outdoor thermal environment would be to modify the thermal and radiative properties (albedo, emissivity, thermal admittance, etc.) of surrounding surface materials. However, the influences of surface materials on T_{mrt} have not been quantified yet.

2.5. Modelling the mean radiant temperature

T_{mrt} is typically estimated on the basis of field measurements or modelling. Because field measurements are costly and time consuming, modelling is a convenient way of obtaining an overview of the spatial T_{mrt} distribution within a city, assessing the impact of specific urban factors, and making predictions about the future thermal environment. Currently, there are a few models for computing T_{mrt}; the RayMan model (Matzarakis et al. 2007; Matzarakis et al. 2009), the SOlar and LongWave Environmental Irradiance Geometry-model (Lindberg et al. 2008) (SOLWEIG) and the ENVI-met (Bruse and Fleer 1998). While the RayMan model calculates T_{mrt} only at a specified place, the SOLWEIG and ENVI-met models simulate its spatial variation. The resulting two-dimensional T_{mrt} distribution reveals hot spots in the urban area, which is very useful in the context of urban planning. According to a model inter-comparison reported by Chen et al. (2014), two-dimensional simulations performed with SOLWEIG are more accurate than those performed with ENVI-met. In addition, the SOLWEIG has been evaluated using data for multiple cities with diverse climates, e.g. Gothenburg, Sweden, Freiburg, Germany and Hong Kong (Lindberg and Grimmond 2011; Chen et al. 2014; Lau et al. 2015).

The calculation of T_{mrt} requires meteorological input variables, which should ideally have been recorded at exactly the location for which the T_{mrt} is to be calculated. However, due to the limited availability of such data, the input data for the model is often obtained from measuring stations that may be some distance from the place of interest (e.g. at the nearest airport). Furthermore, long-term mean values are sometimes used rather than high resolution sequential data. This probably introduces some systematic error into the calculations.

3. METHODOLOGY AND DATA

The studies in this thesis are intended to contribute to the ongoing development of a coupled model system called the Urban Multi-scale Environmental Predictor (UMEP), which is a climate service tool designed to meet the needs of researchers, architects and urban planners (Lindberg et al. 2015). It is intended to be useful in diverse applications related to outdoor thermal comfort, urban energy consumption, climate change mitigation, and so on. An overview of the components developed in this thesis is shown in Figure 2. The modelling work presented in **Papers I** and **II** enables the computation of urban site-specific T_a values, which can be used for the estimation of T_{mrt} and the urban energy balance, respectively. **Paper I** describes the development of the BLUEWS coupled model system, which combines a CBL slab model with a ULSM (two ULSMs are considered, called SUEWS and LUMPS) (Sections 3.1 and 4.1). **Paper II** presents the empirical development of the NOcturnal Cooling RAte Model (NOCRAM) for simulating nocturnal cooling rates, which also enables the calculation of T_a (Sections 3.2 and 4.2). NOCRAM can be used as a replacement for the CBL slab model when computing night-time T_a values. **Paper III** presents an analysis of nocturnal cooling in the near-surface atmosphere under different synoptic weather conditions and seasons (Sections 3.3 and 4.3). The findings support the model concept of NOCRAM and suggest some ways it could be further developed. In **Paper IV**, a ground cover scheme for SOLWEIG was developed to calculate T_{mrt} over different types of ground cover (Section 3.4 and 4.4). The coupling of the models in UMEP will make it possible to obtain some of the input data required by individual models from the outputs of other models, reducing the overall requirement for input data. Specifically, the coupling eliminates the need for experimental data on T_a, relative humidity RH, and sensible and latent heat fluxes (denoted Q_H and Q_E, respectively), making the model applicable in a wider range of applications.

3.1. Modelling of daytime urban site specific air temperatures

Paper I describes the development and evaluation of a coupled model system (BLUEWS) consisting of a CBL slab model and a ULSM. BLUEWS was used to estimate urban site-specific T_a values from measurements recorded at reference stations located elsewhere (e.g. rural sites and airports). This was done by applying a perturbation to the reference T_a before calculating the value at the urban site. In this way, it was possible to account for differences in land cover between the two sites that affect the meteorological measurement of input variables. Urban site-specific relative humidity (RH) values were also calculated in a similar way.

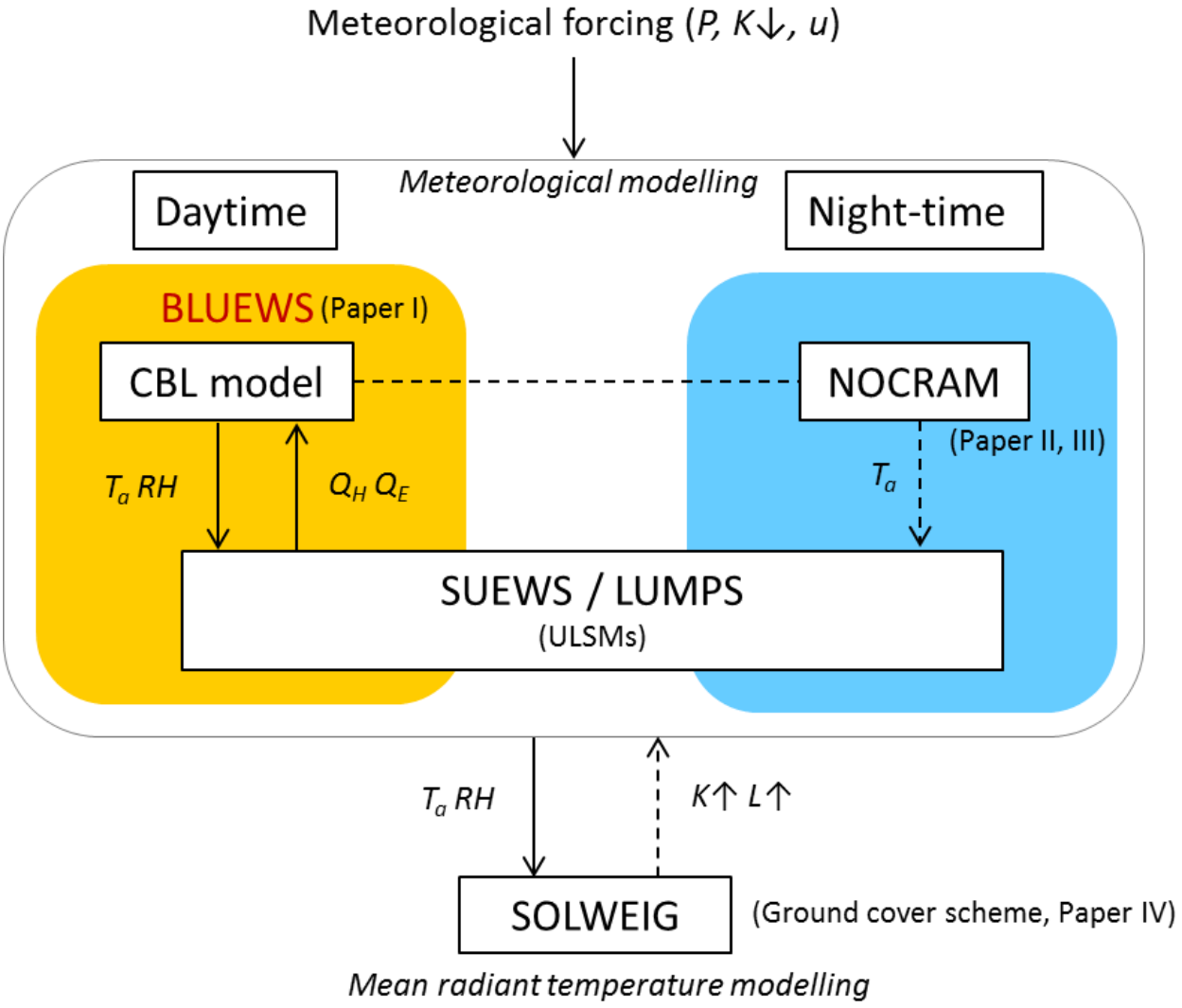

Figure 2. Overview of a coupled model system for predicting selected variables such as air temperature (T_a) and mean radiant temperature. Dashed arrows indicate areas of ongoing work. Abbreviations of model and variable names are found in text and in the abbreviation list.

In the developed model system, the CBL slab model calculates temporal changes in potential air temperature (θ), specific humidity (q) and the height of the CBL (z_i) using the equation of heat and water vapour conservation with the Tennekes and Driedonks (1981) entrainment scheme. The CBL model requires data on Q_H and Q_E. Two ULSMs were used to determine the surface fluxes: the Surface Urban Energy and Water balance Scheme (SUEWS) (Järvi et al. 2011) and the Large-scale Urban Meteorological Parameterization Scheme (LUMPS) (Grimmond and Oke 2002; Loridan et al. 2010). An important difference between the two is that SUEWS evaluates surface resistance using the Penman-Monteith approach and is thus a biophysical method, whereas LUMPS uses the de Bruin and Holtslag (1982) simplification of Penman-Monteith to calculate Q_H and Q_E. Both models require land cover information and data on meteorological variables such as T_a, RH, the incoming shortwave radiation ($K\downarrow$), wind speed (u), and air pressure (P) at the local scale (above the RSL). In addition, both models compute the other flux components of the urban SEB such as the net-all wave radiation flux, anthropogenic heat flux and

storage heat flux. The two ULSMs were coupled in parallel to the CBL slab model. For the sake of simplicity, the CBL + SUEWS model is henceforth designated BLUEWS while the CBL + LUMPS model is henceforth referred to as BLUMPS. Coupling the models in this way enables the CBL model to compute θ and q using Q_H and Q_E values from one of the ULSMs, while the ULSM can estimate surface heat fluxes using T_a and RH values derived from the θ and q values generated by the CBL in the previous time step (Figure 3). Consequently, the need for input data on T_a, RH, Q_H and Q_E is eliminated; the only forcings relevant to the combined model are $K\downarrow$, P and u. However, the CBL model can only be used to model daytime conditions. In addition, the model requires forcing data including initial values of θ, q and z_i as well as the vertical gradients of θ and q just above the CBL to enable the estimation of the net fluxes from the entrainment zone as well as the CBL growth. The detailed formulas used in these models are given in **Paper I** and elsewhere (Cleugh and Grimmond 2001; Järvi et al. 2011).

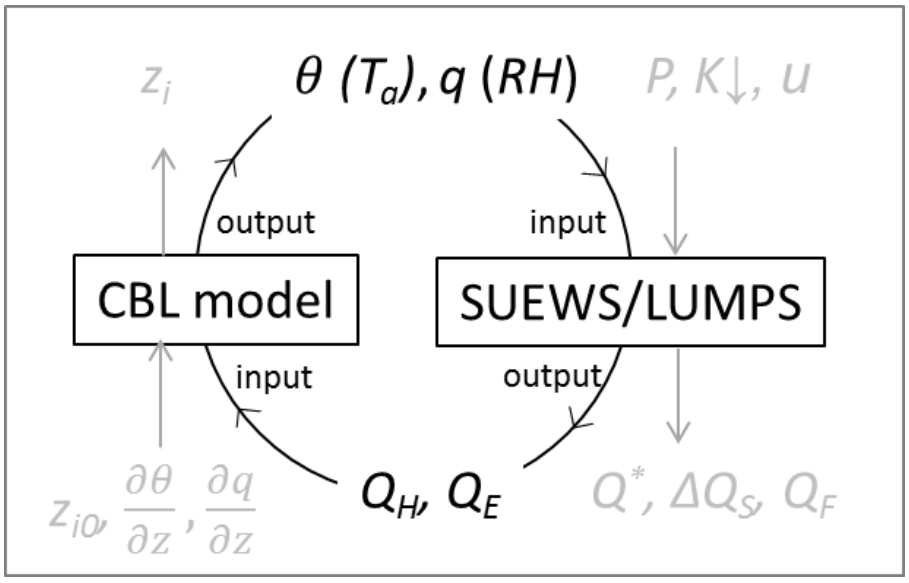

Figure 3. Core structure of BLUEW (BLUMPS) model showing the forcing input data and outputs (both in grey) of the coupled CBL and SUEWS (or LUMPS) models, as well as the variables linking the two constituent models (i.e. θ, q, Q_H and Q_E). Figure source: Paper I.

Meteorological data (T_a, RH, u, P, Q_H, Q_E, etc.) measured at a suburban site and a dry site in Sacramento, California, U.S.A. between 20th and 29th August 1991 (Grimmond et al. 1993; Grimmond and Oke 1995) were used to evaluate the BLUEWS and BLUMPS models and assess their usefulness for estimating urban site-specific T_a values. Importantly, the reference data set included measurements of θ and q within the CBL for the 22nd –24th and 26th – 28th August, which were acquired using free-flying radiosondes released at the suburban site (Cleugh and Grimmond 2001). z_i was estimated as a height at which θ was inverted.

3.2. Modelling of night-time urban site specific air temperatures

Paper II describes the development of the NOcturnal Cooling RAte Model (NOCRAM) for calculating nocturnal cooling rates and T_a at 2 m above the ground within urban areas. This model is based on the two-phase cooling concept established in earlier works, e.g. Acevedo and Fitzjarrald (2001), Acevedo and Fitzjarrald (2003) and Holmer et al. (2007). Figure 4 shows a typical cooling rate profile for an open site under ideal (cool and calm) conditions in which the two distinct cooling phases (Phases 1 and 2) are clearly visible, along with the subdivision of Phase 1 into Phases 1A and 1B. Phase 1A and 1B were modelled with different cosine functions taking as their inputs the initial cooling rate (CR_1) of Phase 1A, the most intensive cooling rate (CR_{peak}), the initial cooling rate (CR_2) of Phase 2 and the timings of Phases 1A, 1B and 2 (t_1, t_{peak} and t_2). CR_1 was determined from observed T_a values. t_{peak} was simply calculated as the mean of t_1 and t_2, even though it was found in this study that t_{peak} was probably predicted by changes in the atmospheric stability. Phase 2 was modelled with a linear function using CR_2 and t_2 under the assumption that cooling ends at sunrise (= t_{end}). Finally, the profile was modified to account for the effects of wind disturbances on cooling rates, which were computed at each time step taking as parameters the wind speed and atmospheric stability.

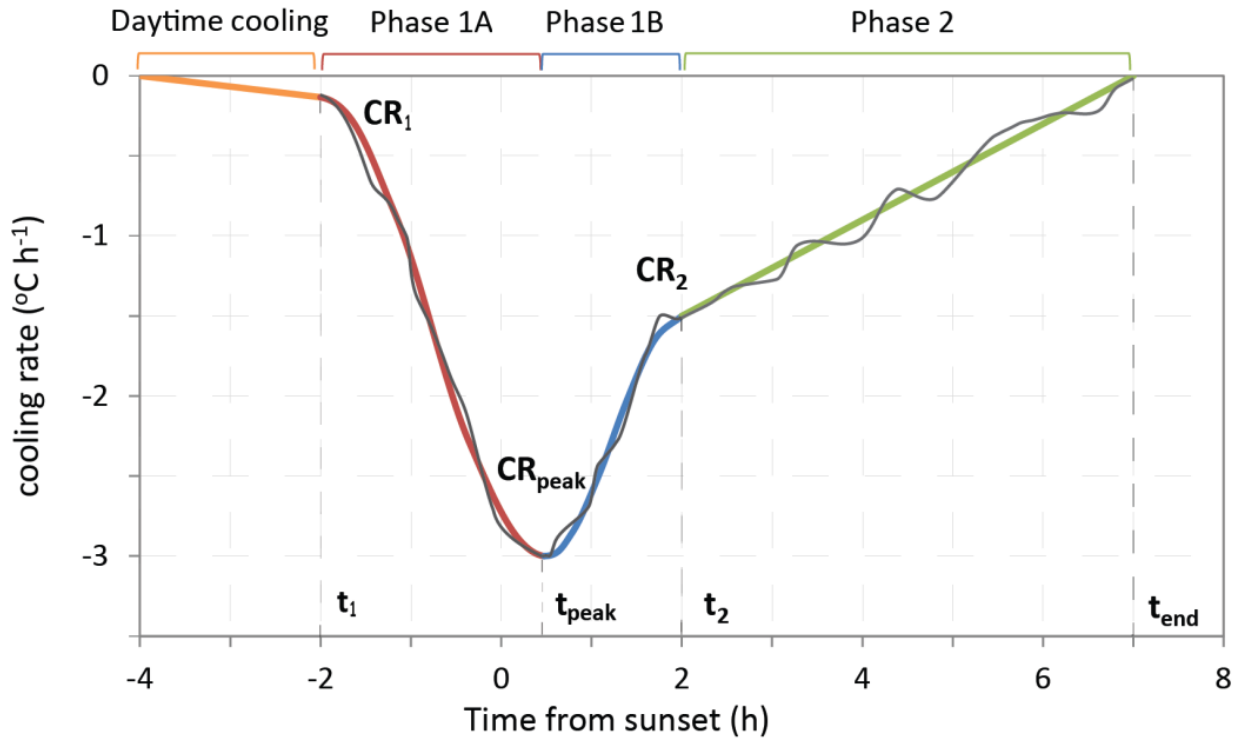

Figure 4. A representative cooling rate profile for an open site under ideal (clear and calm) conditions. The start and end of Phases 1A, 1B and 2 are indicated by t_1, t_{peak}, t_2 and t_{end}, respectively. The initial cooling rate in Phase 1A (CR_1), most intensive cooling rate (CR_{peak}) and initial cooling rate in Phase 2 (CR_2) are shown. A thin oscillating line around the profile illustrates how weather changes such as wind and cloud cover/type affect cooling rates during the night. Figure source: Paper II.

To resolve the expressions mentioned above, it was necessary to determine t_1, t_2, CR_{peak} and CR_2. The timings of t_1 and t_2 were determined by the times of daytime large-scale turbulence decay and turbulence breakdown, respectively. These changes in turbulence structure were detected by their effects on wind speed. CR_{peak} was estimated by first considering the impact of the prevailing weather conditions (which were assessed in terms of clearness index of the sky, *CI* and the wind speed, U_1), seasonality (indicated by the maximum daily air temperature, T_{max}) and then accounting for the impact of the site's urban density (represented by the sky view factor, *SVF*). The impact of *CI* and U_1 was parameterized by introducing a new weather factor, the Cooling Rate Impact Factor (*CRIF*, Figure 5), which expresses various cloud and wind conditions and takes values ranging from 0 (cloudy and windy) to 1 (clear and calm). Classifying the data using the *CRIF* simplified the parameterization of the influence of T_{max} and *SVF* on CR_{peak}. CR_2 was determined by the intensity of thermal stratification of the stable atmosphere (indicated by *CI*) and the strength of vertical mixing (wind speed at t_2). Note that NOCRAM deals with local weather changes (with the exception of precipitation) and cannot account for larger-scale weather changes. In addition, it cannot currently account for the effects of evapotranspiration and anthropogenic heat on cooling rates. The determination of the quantities discussed above is described in detail in **Paper II**. As inputs, the model requires only standard meteorological variables (i.e. u, $K\downarrow$, daytime T_a, *RH* and *P*) measured at a reference station and geometric information (i.e. the SVF of the site and the geographical co-ordinates of the reference station).

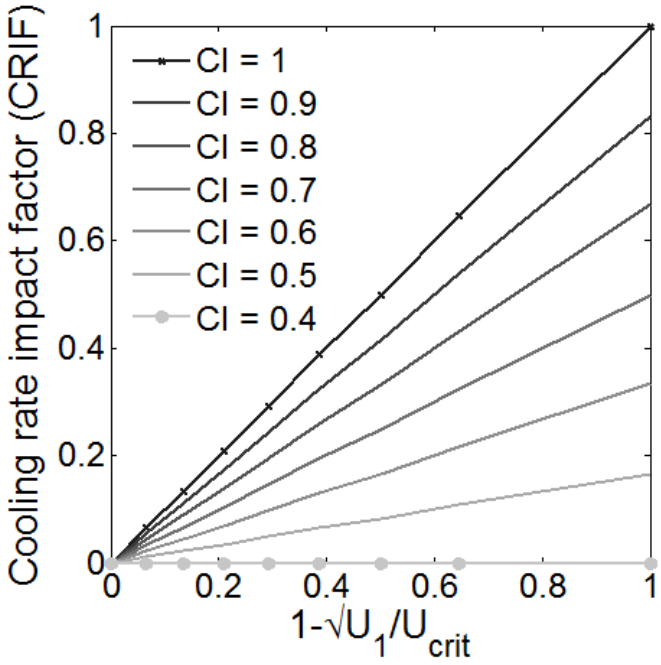

Figure 5. The variation of the cooling rate impact factor with the clearness index of the sky (*CI*) and average wind speed (U_1) for ± 3 hours around the time of most intensive cooling. The critical wind speed (U_{crit}) is set to 4 m s^{-1}. Figure source: Paper II.

The model was developed using a reference meteorological dataset (Thorsson and Eliasson 2003) containing T_a values measured between May and September in 1999 at an open site (*SVF* = 0.98) and in a narrow street (*SVF* = 0.39), both with little vegetation, in the city centre of Gothenburg. *u* was measured at 10 m at the open site while *K*↓, *RH*, *P* and precipitation data were taken from other meteorological stations around the open site. The clearness index of the sky was calculated as the ratio of the measured solar irradiance to the clear-sky irradiance (Crawford and Duchon 1999; Lindberg and Grimmond 2011) but only daytime data on this variable were available. Therefore, the night-time *CI* was calculated as the average clearness index of the sky across the night. Two independent datasets were used to evaluate the model, one from Gothenburg and one from London. The Gothenburg dataset consisted of T_a measurements for an open site (*SVF* = 0.92) and a built-up site (*SVF* = 0.40) covering the period of May to September in 2012 and 2013 (Konarska et al. 2015). The London dataset consisted of T_a measurements at a built-up site (*SVF* = 0.46) in a complex urban setting with substantial variation in building height during the period of June to September in 2014. The *SVF* is the average *SVF* of the ground surface within a 25 m radius, calculated using a digital surface model of buildings and vegetation (Lindberg and Grimmond 2010).

3.3. Analysis of the vertical distribution of nocturnal cooling

Paper III presents an analysis of nocturnal cooling rates measured at six heights (3, 14, 56, 75, 83 and 105 m) along a 105 m tall tower at Järnbrott in Gothenburg. The tower is located in a suburban area featuring buildings of 2-3 stories, parks and woodlands. The mean building and vegetation height of the surroundings was estimated to be 7.3 m using a digital surface model of the buildings and vegetation. T_a was measured with PT100 thermometers and differential thermometers, and the T_a dataset was calibrated *in situ*. Local weather conditions were characterized by *u* measurements acquired at two heights on the tower (16 and 105 m) and night-time bulk *CI* calculated using the method described in Section 3.2. *K*↓ were measured at the same study site, and *P* and *RH* were taken from another weather station in the city. The bulk Richardson number (Ri_b), an atmospheric stability index, at geometric heights of 6.5 and 78.8 m was estimated according to the equation of Golder (1972). All of the data used in the analysis have a time resolution of one hour and were gathered between January 2005 and July 2013.

The data were divided into groups according to the prevailing synoptic atmospheric circulation patterns, which were assigned on the basis of the Lamb Weather Type (LWT) system (Lamb 1950). LWTs over Gothenburg were obtained by computing six hour average sea level pressures for 16 grid points centred at 57°7´N, 12°5´E using the NCEP/NCAR reanalysis database 2.5×2.5 degree pressure fields (Kalnay et al., 1996). The detailed procedure for determining the LWTs was explained by Chen (2000). Atmospheric circulation patterns were classified into 27 weather types: anti-cyclonic (A),

cyclonic (C), eight directional flow types (N, NE, E, SE, S, SW, W and NW), 16 hybrid types (e.g. AN, ASE, CS and CNW) and undefined pattern (UD). LWTs were determined at six hour intervals, starting at midnight, in the study period This made it possible to detect recurring LWT patterns between the 12:00 and 06:00 (all times given are in UTC), i.e. during the period when nocturnal cooling occurs. In addition to being grouped according to the prevailing LWT, the data were divided seasonally.

3.4. Development of a ground cover scheme in SOLWEIG

Paper IV describes the development of a ground cover scheme in SOLWEIG (Lindberg et al. 2008) for different types of ground cover (asphalt and grass) and its use to assess the impact of changing the ground surface types on T_{mrt}. SOLWEIG derives T_{mrt} by separately computing short- and long-wave radiation fluxes from six directions. The T_{mrt} is generally calculated at a height of 1.1 m, corresponding to the position of a standing person's center of mass. At minimum, the model requires input data in the form of weather time-series (at any time resolution) for T_a, RH and $K\downarrow$, together with a digital surface model and the site's geographical location (i.e. latitude, longitude, and altitude). The ground cover scheme modifies the upward shortwave and long wave radiative fluxes based on the characteristics of the ground cover.

In SOLWEIG, the upward shortwave radiative flux for a pixel within a model domain is calculated as the sum of the single reflections of direct and diffuse radiation and the second reflection of radiation from the surroundings such as buildings and vegetation on the ground surface (eq. 16 in **Paper IV**). The different types of the ground cover modify the albedo values for each pixel on the ground surface.

Throughout the model domain, the upward long wave radiative fluxes are estimated, mainly on the basis of the surface temperature, T_a and ground emissivity. The surface temperature is estimated using the method of Bogren et al. (2000), which assumes a linear relationship between the maximum solar elevation and the maximum air-surface temperature difference. The robustness of this approach was evaluated using data for a cobbled stone surface under clear and calm conditions, which is the only type of surface previously considered using SOLWEIG (Lindberg et al. 2008). To simulate other surface materials, it was necessary to derive suitable linear relationships. Therefore, surface temperatures were measured for two different surfaces (dark asphalt and short grass) in an open field adjacent to Gothenburg City Airport from 1st July 2011 – 31st December 2012. Infrared radiometers (Apogee, SI-111) were positioned 0.5 m above the ground surface, looking vertically downward. The resulting relationships for the two surface types (Figure 3 in **Paper IV**) were incorporated into the ground cover scheme. In addition, a simplification was introduced whereby the surface temperature at shadowed locations was assumed to be equal to T_a. Modified emissivity values for each surface type were also incorporated into the model.

To evaluate the new SOLWEIG ground cover scheme, T_{mrt} and surface temperatures were recorded at a site with a well-maintained grass lawn and another site with a dark tile surface at the Barbican Estate in London, UK during the summer of 2014. The base of the grass site was a silty loam and the dark tile site was located in an elevated playground belonging to a school. The T_{mrt} measurements were acquired by using a mobile station consisting of three net radiometers (Kipp & Zonen, CNR 1) mounted on a steel stand to measure the 3-D shortwave and longwave radiation fields (Thorsson et al. 2007). Surface temperatures were monitored using additional infrared sensors of the same kind, which were also attached to the mobile station. T_a and *RH* were measured with a Rotronic HydroClip2 (HC2-S3) instrument. In total, measurements were taken over four days at the grass site and six days at the dark tile site. All data were averaged over 15 minute intervals, which is the resolution of the model runs.

The ground cover scheme was evaluated using a simplified version of SOLWEIG called SOLWEIG1D (Lindberg 2012). SOLWEIG1D calculates radiation fluxes and T_{mrt} for a generic location within an urban environment with a user-specified *SVF*. The location is assumed to be sunlit at all times during the day.

4. RESULTS

4.1. Evaluation of modelling of daytime urban site specific air temperatures

The coupled model system (BLUEWS and BLUMPS) was developed. Their performances for z_i, θ and q were evaluated using observations from the suburban site in Sacramento as well as in comparison with the CBL results of Cleugh and Grimmond (2001) (Figure 6). All runs show good overall performance. For some days, the variables modelled by BLUEWS and BLUMPS agree with the observation better than the results of Cleugh and Grimmond (2001). This means that the coupling of these models does not deteriorate the CBL model performance. Given that BLUEWS performs better than BLUMPS for q, the results support the use of the biophysical evaporation model SUEWS. In addition, BLUEWS and BLUMPS were run for the dry site (Figure 6 in **Paper I**). The larger growth of z_i and θ and decreasing q due to larger Q_H and smaller Q_E compared to the suburban site were modelled. This clearly shows that land surface characteristics significantly influence the properties of the CBL.

Representative T_a and RH values for the suburban area were obtained by perturbing the corresponding values for the dry site using BLUEWS and BLUMPS (Figure 7). The predicted suburban T_a and RH values correlated well with the observations, with RMSE values of 1.3 ˚C and 6.2 % being achieved for T_a and RH, respectively, using BLUEWS. Although the absolute RMSE value of RH is greater than that of T_a, sensitivity tests showed that the accurate prediction of T_{mrt} with SOLWEIG is much more heavily dependent on the accuracy of the input T_a than on that of RH (Section 5.1. in **Paper I**).

This new system showcases the potential for improving the modelling of T_{mrt} by using meteorological variables that are more representative of urban sites in place of data from non-urban sites.

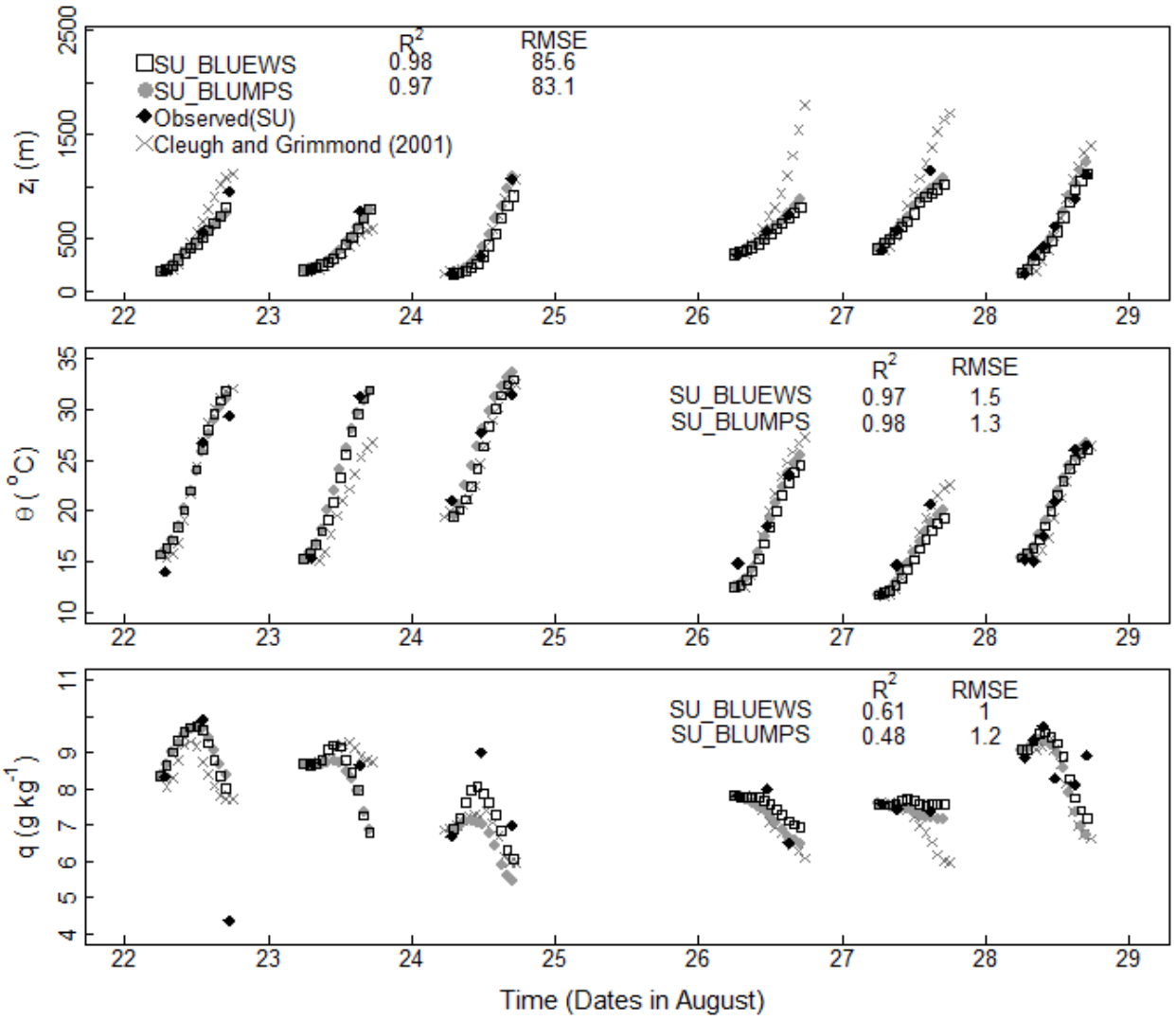

Figure 6. Modelled convective boundary layer heights (z_i), potential temperatures (θ) and specific humidity values (q) for suburban Sacramento on the 22nd - 28th August, 1991, using the coupled models (BLUEWS and BLUMPS). The results of Cleugh and Grimmond (2001) and radiosonde observations are shown for comparative purposes, and the modelled results are plotted hourly. Figure source: Paper I (modified).

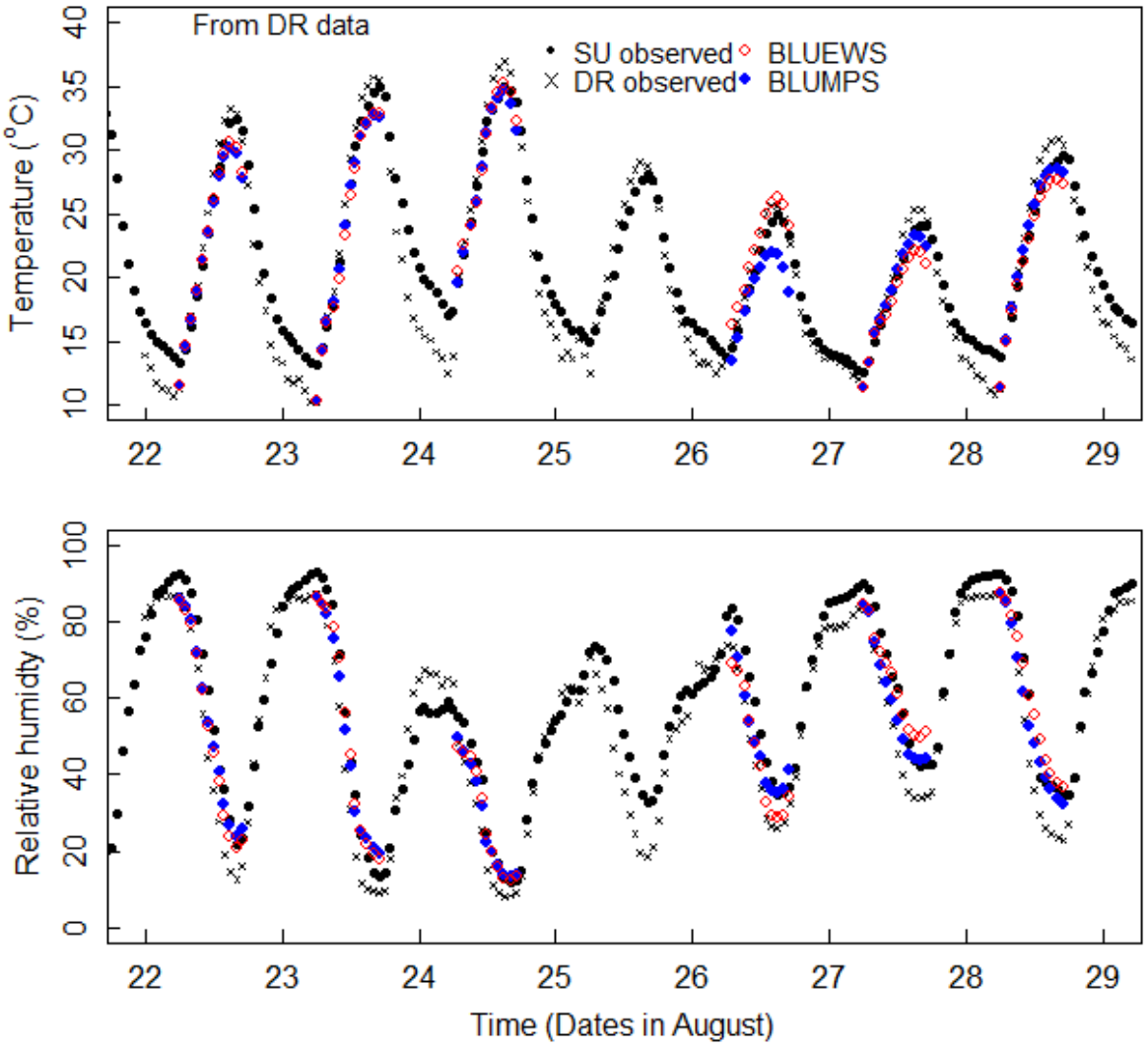

Figure 7. Suburban air temperature and relative humidity modelled by perturbation of data for a dry rural site using coupled models (BLUEWS/BLUMPS) in comparison to observations at suburban (SU) and dry rural (DR) sites. Figure source: Paper I.

4.2. Evaluation of modelling of night-time air temperatures

Time series of modelled and observed cooling rates, T_a values, wind speeds, and wind directions covering two days (28th of July and 22nd of June 1999) at an open site (*SVF* = 0.98) were studied (Figure 8). The figure also shows the observed cooling rates for a built-up site (*SVF* = 0.39) to indicate the start timings of Phase 1 and Phase 2 (t_1 and t_2), and the points at which the cooling rates at the urban and open sites diverge and converge. A typical cooling profile with two distinct phases was observed on the 28th of July (Figure 8, left), when the conditions were clear and calm. In this case, the model simulates the temporal development of cooling rates reasonably well. The magnitude of CR_{peak} is also reasonably modelled. The predicted timings of t_1 and t_2 agree with the observations, but t_{peak} appears half an hour later than was observed. This could be due to the simplified method that t_{peak} is calculated as the mean of t_1 and t_2. Regardless, the characteristics of the intensive cooling during Phase 1 are well captured. The model is particularly successful at simulating the variations in cooling rates caused by wind disturbance during Phase 2. On the other hand, the model does not capture the observed cooling that occurred on the 22nd of June (Figure 8, right); it either overestimated or underestimated the cooling rates in Phases 1B and 2. The observations show that the point at which the wind speed falls to near-zero and the wind direction changes from west to east (from a sea breeze to a land breeze) occurred rather late at night on the 22nd. The wind speed increased around four hours after sunset and shortly thereafter the observed cooling at both the open and built-up sites increased strongly, probably as a consequence of a change in the synoptic weather conditions. This may explain why the model could not provide reliable predictions on this occasion: it is only applicable under steady synoptic weather conditions.

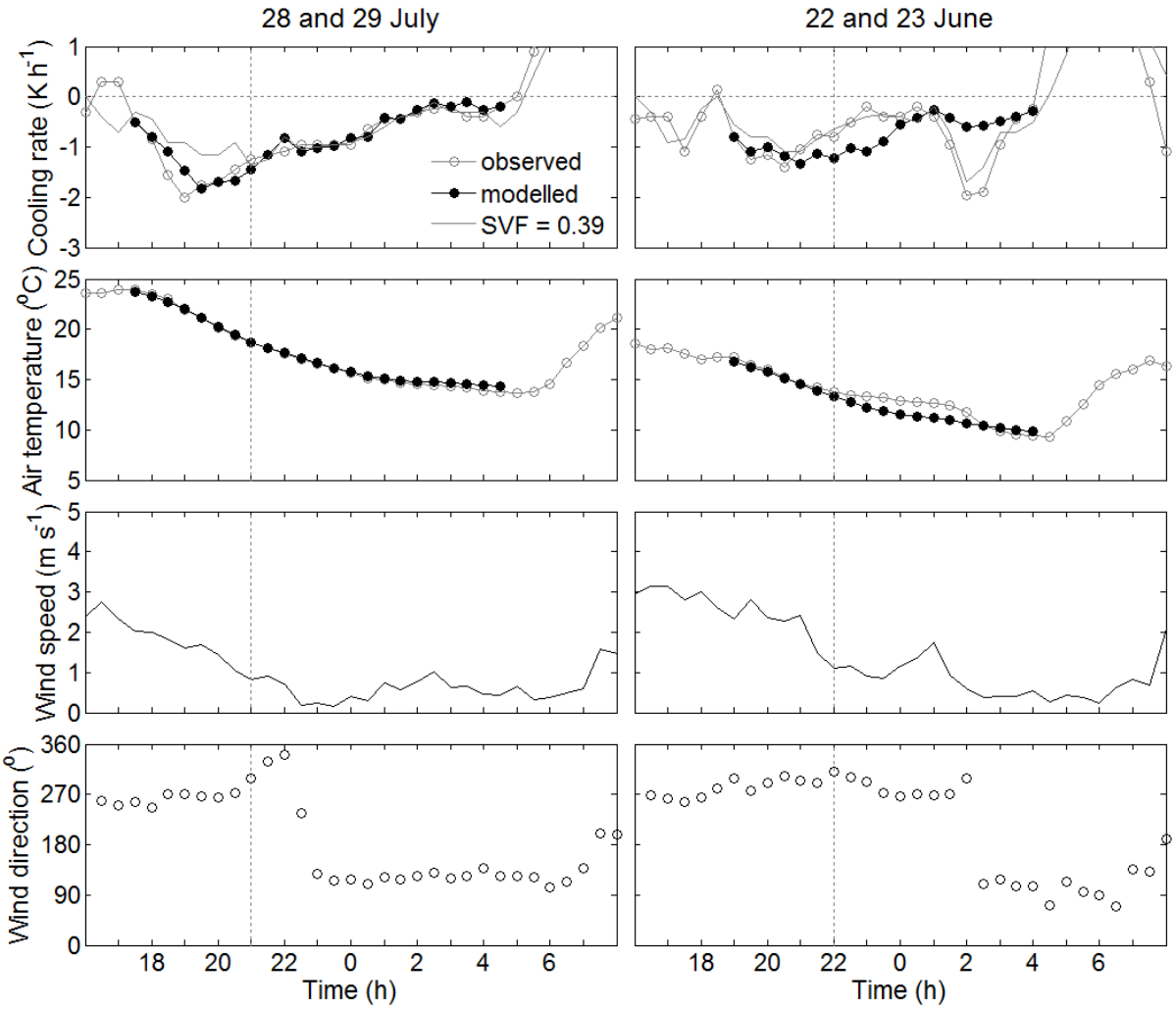

Figure 8. Nocturnal profiles of modelled (black dot) and observed (grey circles) cooling rates, air temperatures, wind speeds (black line) and wind directions for the 28th of July, 1999 at an open site (SVF = 0.98) in Gothenburg. Measured cooling rates for a built-up site (SVF = 0.39) are also presented in the cooling rate plots to show the start timings of Phases 1A and 2 when cooling rates at the two sites diverge and converge, respectively. A vertical dashed line indicates sunset. Figure source: Paper II (modified).

Figure 9 shows mean modelled and observed cooling rate profiles for two open sites (*SVF* = 0.98 and 0.92) and three dense sites (*SVF* = 0.39, 0.40 and 0.46) under the three weather conditions corresponding to the 25^{th} percentile of *CRIF*, the inter-percentile and the 75^{th} percentile. These three classes correspond roughly to clear and calm (ideal) conditions, semi-cloudy and light-wind conditions, and cloudy and windy conditions, respectively. The datasets for the sites with *SVF* values of 0.92, 0.40 and 0.46 were independent and not used in the model's development. The model predicted the cooling rates for all sites reasonably well. The standard deviations (shown by vertical bars) indicate the daily variation in the cooling rates, which are similar in magnitude and show similar patterns for both the model's predictions and the observations. The profile of the open site (*SVF* = 0.98, first column) clearly shows that the modelled cooling rates under clear and calm conditions are substantially greater than those for cloudier and windier conditions. In addition, the two cooling phases become less distinct as the conditions become cloudier and windier. Statistical analysis of the model's performance (Table 1, in **Paper II**) revealed slight positive mean bias errors (~ 0.06 K h^{-1}), indicating that the model tends to underestimate cooling rates. The model correctly predicts that the Phase 1 cooling rates at a built-up site (*SVF* = 0.39, third column) are lower than those for the open sites under all weather conditions. Overall, the model's statistical performance for the urban site is almost identical to that for the open site. The modelled cooling rates for the independent sites in Gothenburg and London (i.e. *SVF* = 0.92, 0.40 and 046) are also in good agreement with the corresponding observations. Moreover, the model's statistical performance for these sites is slightly lower than that for the *SVF* = 0.98 and 0.39 sites. Nevertheless, it appears that the model can simulate cooling rates reasonably well at independent sites as well as sites with complex urban geometries and in other cities with similar climate zones.

Air temperature calculated using the modelled cooling rates corresponds with the observations (not shown). The statistical performance is RMSE $\leq$ 1.54 ˚C and mean bias error $\leq \pm$0.7 ˚C (Table 1, in **Paper II**).

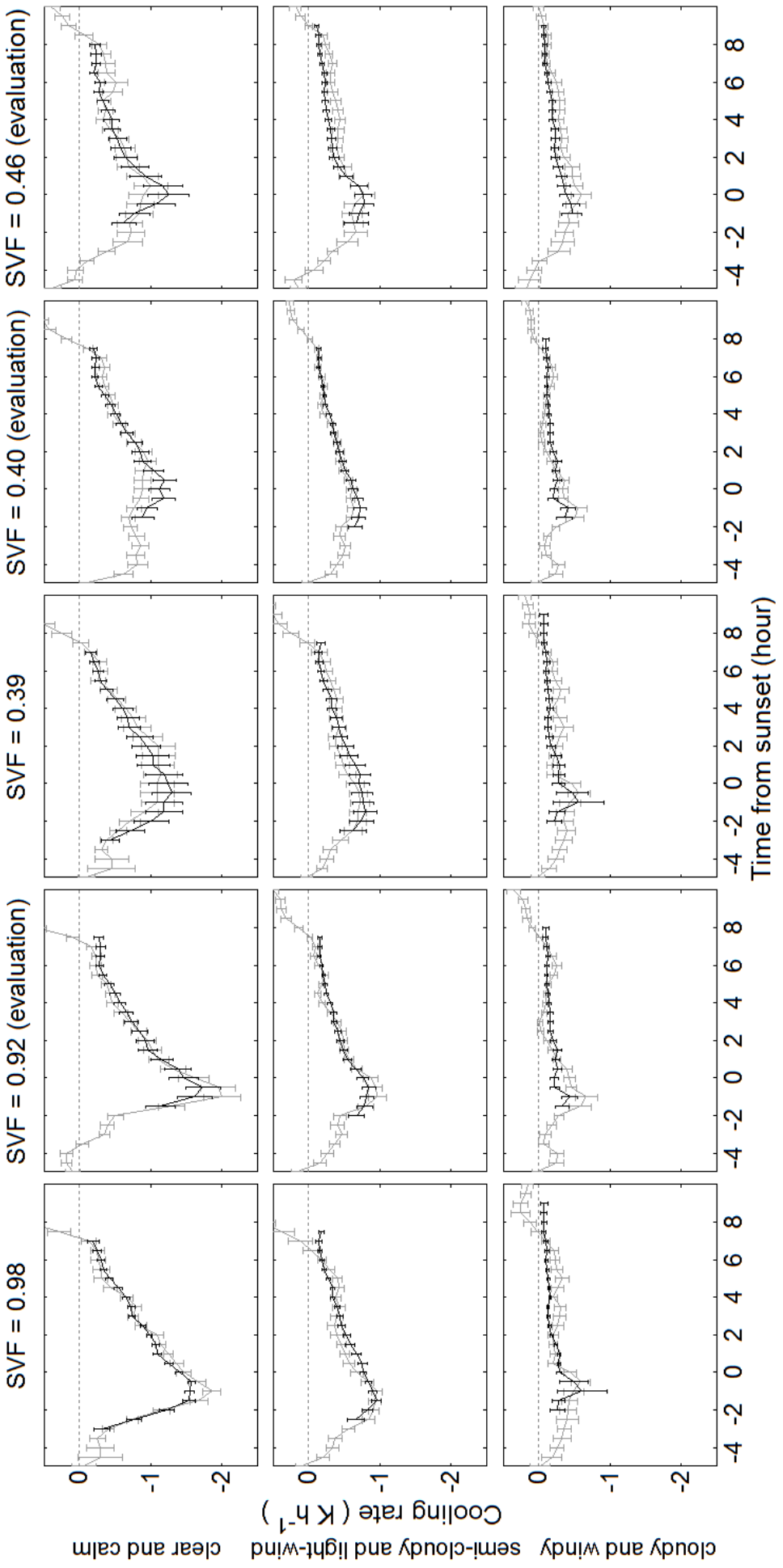

Figure 9. Average modelled (black) and observed (grey) cooling rate profiles for two open sites (*SVF* = 0.98 and 0.92) and two built-up sites (*SVF* = 0.39 and *SVF*= 0.40) in Gothenburg, and one built-up site (*SVF* = 0.46) in London for three weather conditions (upper row: clear and calm conditions, middle: semi-cloudy with light wind, lower: cloudy and windy), classified by the cooling rate impact factor (25^{th} percentile, 25^{th} – 75^{th} percentile, 75^{th} percentile). For the different lengths of night between May and September, the modelled cooling rates were plotted

4.3. Vertical distribution of nocturnal cooling rates under different synoptic weather conditions

LWT types were examined during the period between 12:00 and 06:00 over the site in Gothenburg. On 27% of the total study days, the LWT did not change during this period. Ten major LWTs detected (see Figure 2 in **Paper III**) also exhibit the trend in most cases. The ten major types were divided into four groups; anti-cyclonic conditions (A), cyclonic conditions (C), westerly or south-westerly directional flows (W+SW), and north-westerly, southern, south-easterly or easterly directional flows (NW+S+SE+E). Average cooling rate profiles for each group at six heights (3, 14, 56, 73, 85 and 105 m) are shown in Figure 10.

The A group exhibits that maximum cooling is reached within a narrow temporal window around sunset at all heights and that cooling is more intensive near ground. Two layers are readily apparent in the nocturnal cooling development: intensive cooling occurs with large height-dependent variations at three lowest elevations (3, 14 and 56 m) and the rates of cooling are much lower at the three higher elevations (73, 85 and 105 m). In both layers, cooling can be divided into two phases because of clear differences in the cooling process. In the lower layer, the cooling rates vary with height around sunset (Phase 1) but converge three hours after sunset (Phase 2). Conversely, in the upper layer the cooling rates gradually diverge in Phase 1 and the differences between heights persist in Phase 2. This implies that different cooling processes occur in the lower and upper layers. Interestingly, the timings of the two phases found in this analysis roughly correspond to those of the two phases proposed by Holmer et al. (2007) based on the spatial differences in cooling rates. A similar two-layer pattern was observed in the cooling rate profile for the other LWT pattern groups.

Group C exhibits substantially lower cooling rates than group A. As with group A, the two layers appear and the cooling rate decreases as the height increases. Two distinct cooling phases are observed at all heights, but the differences between the phases are much less pronounced than is the case for group A. The height-dependent variation in the upper layer is very modest. The W + SW group exhibits substantially weaker cooling than group C. The two layers appear only during Phase 1 but converge in Phase 2. Two separate cooling phases can be distinguished in the lower layer but not in the upper layer. Finally, the NW+S+SE+E group exhibits more or less the same cooling development as group C in terms of the magnitude of cooling and its height-dependent variation.

The characteristic development of nocturnal cooling, with two layers and two phases, also varies between seasons (Section 3.2 and Figure 4 in **Paper III**). The pattern is most pronounced in spring, followed by summer and autumn under anti-cyclonic conditions but less apparent in winter under anti-cyclonic conditions and during all seasons under

cyclonic and directional flow conditions. The same is true for the magnitude of the cooling rates.

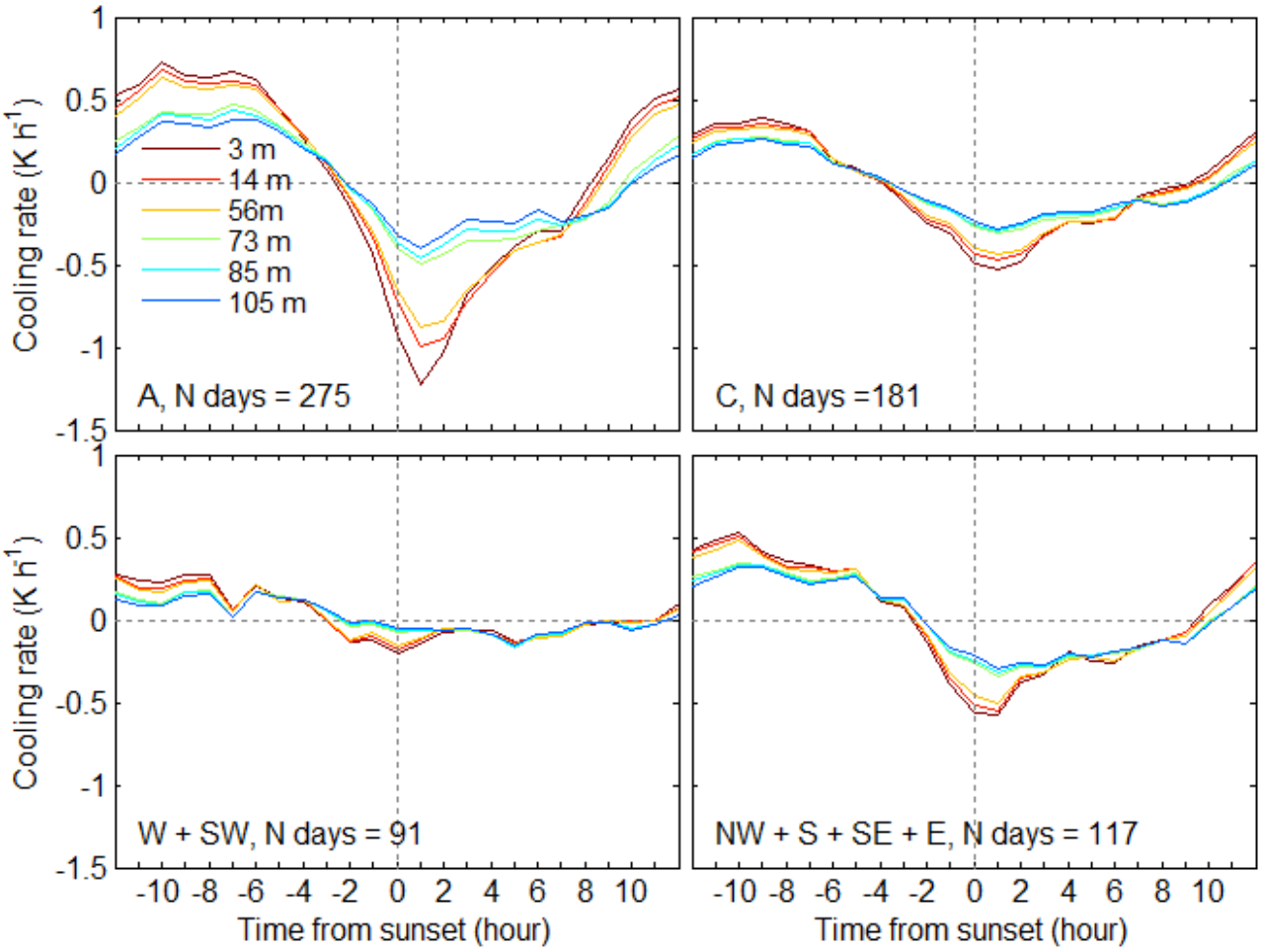

Figure 10. Average cooling rate profiles for four nocturnal Lamb weather type patterns (A, C, W+SW, NW+S+SE+E) covering the period from 12:00 to 06:00 during 2005-2013. The number of days of data used to construct the average profiles are shown (N days). Figure source: Paper III.

Average Ri_b values for Phases 1 and 2 at two geometric heights (6.5 and 78.8 m, located in the lower layer and the upper layer, respectively) under anti-cyclonic conditions are shown in Figure 11. In Phase 1, the average Ri_b at 6.5 m (Figure 11, lower-left) is mostly positive, indicating stable atmospheric conditions, while the average Ri_b at 78.8 m (Figure 11, upper-left) is more or less zero, indicating neutral conditions. The average Ri_b in Phase 2 (Figure 11, right) is overall higher than in Phase 1 for the two heights. In particular, significant increases in Ri_b are observed at 78.8 m. This indicates that the atmospheric stabilization evolves in the upper layer on going from Phase 1 to Phase 2. In turn, this implies that during Phase 2 the atmosphere can be stabilized in a layer as deep as the upper layer range, i.e. up to 105 m, under anti-cyclonic conditions. Although the average Ri_b at 6.5 m is higher in Phase 2 compared to Phase 1, the temporal development of Ri_b at 6.5 m shows that the value decreases rapidly within a few hours after sunset (Figure 4 in

Paper III). This process appears to be driven by the stretching of the strongly stabilized air towards the upper atmosphere via long-wave radiative heat exchange. The radiative heat exchange also explains the persistent height-dependent variations in cooling rates in the upper layer in Phase 2. The strength of the atmospheric stabilization exhibits strong seasonal variation at both heights: the atmosphere is considerably stabilized in the warm months but can be weakly stabilized or neutral in the cold months.

Under cyclonic and directional flow conditions, the average Ri_b at the both two heights is approximately zero in Phase 1 (not shown, but see Figure 8 in **Paper III**). In Phase 2, the Ri_b remains close to zero but the Ri_b at 6.5 m can be quite high on some occasions in May, July and August. This implies that the atmosphere in the lower layer could be stabilized in the warm months even under cyclonic + directional flow conditions. However, in the upper layer, neutral conditions are expected.

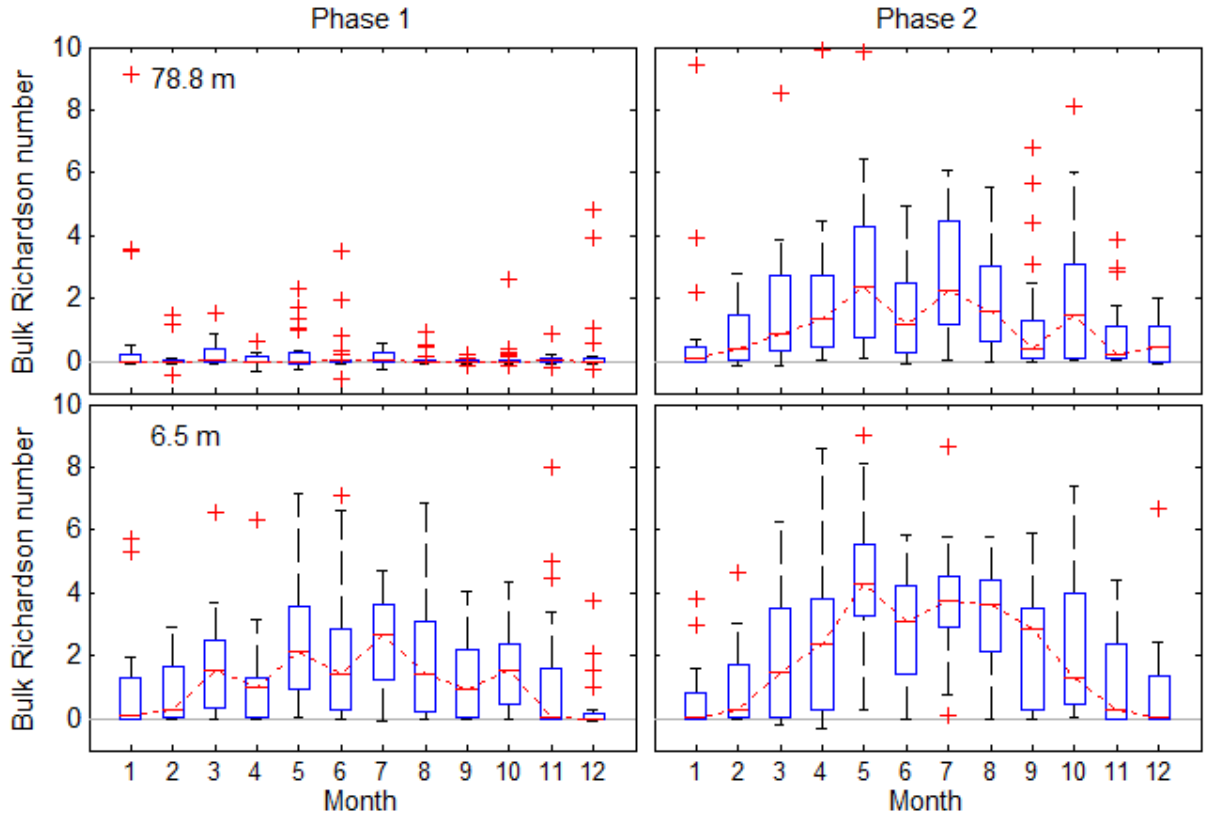

Figure 11. Average bulk Richardson number for ± 1 hour around sunset (left, Phase 1) and from 4 hours after sunset to 1 hour before sunrise (right, Phase 2) at geometric heights of 78.8 m (upper) and 6.5 m (lower) under anti-cyclonic conditions in Gothenburg for each month during 2005-2013. The bottom and top edges of the boxes shows the 25th and 75th percentiles of the data and the lines in the boxes indicate the medians.

4.4. Influence of ground cover types on mean radiant temperature

The ground cover scheme in SOLWEIG was developed to account for different ground cover types. It is now possible to simulate their influences on the radiant fluxes as well as T_{mrt} using SOLWEIG. The surface temperature of different ground surfaces (grass, dark asphalt and cobble stone) for a location in Gothenburg, Sweden with an *SVF* of 0.60 was simulated for a day with clear skies (Figure 12, left). The simulated daytime surface temperatures for the sunlit locations are predicted to be lower for areas with grass surfaces and higher for those covered with dark asphalt when compared to the cobblestoned area simulated by Lindberg et al. (2008). The model simulates the evolution of the surface temperature reasonably well for the three cover types. The surface temperature at the shadowed location (which is assumed to be equal to T_a) at mid-day is approximately 10 °C lower than that of the grassy surface. With respect to differences in T_{mrt} (Figure 12, right) over the different surface types, the largest discrepancies from the model of Lindberg et al. (2008) are found for the grass surface (-5.2 °C at 4 pm); the differences between the cobblestones and dark asphalt are smaller (+1.5 °C at 4 pm). The variation of T_{mrt} over different ground surfaces in sunlit locations is very small compared to the difference between any sunlit location and a shadowed location (-38.2 °C at 4 pm).

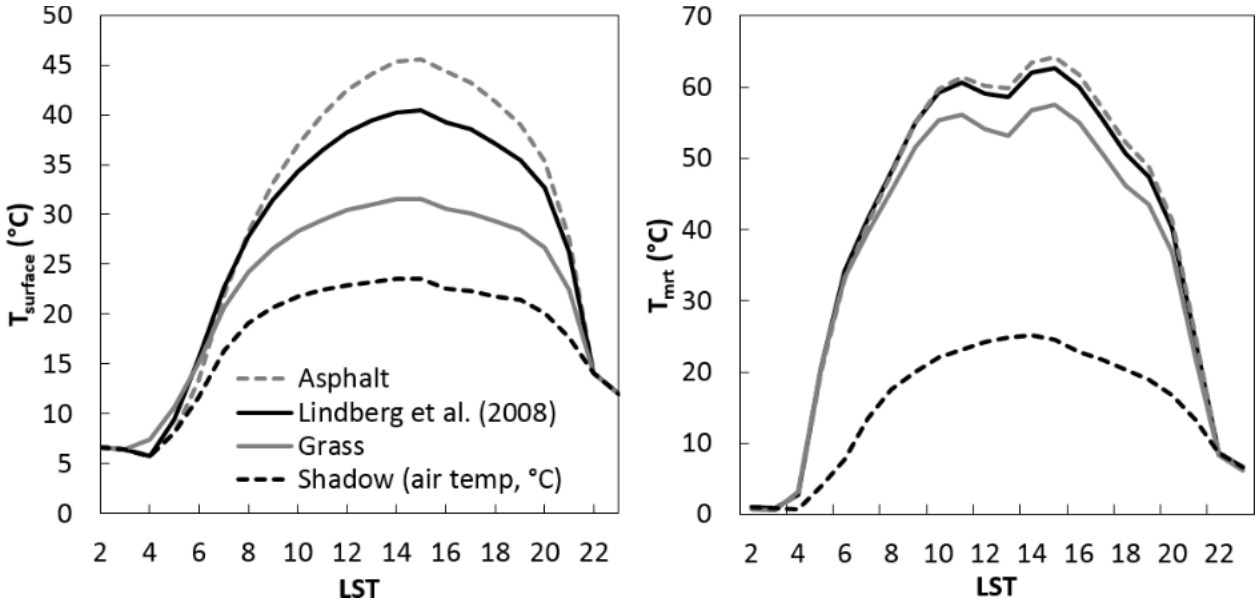

Figure 12. Influence of different ground cover types (dark asphalt, grass, and cobblestones indicated by Lindberg et al. 2008) on the modelled surface temperature (left) and mean radiant temperature (right) on the 6th of June, 1997 in Gothenburg (Sweden). The location is assumed to be fully sunlit with an *SVF* of 0.60. Simulated data for a shadowed location are also shown.

T_{mrt} values computed with the new ground cover scheme were compared to observations made in London. The modelled T_{mrt} values for the dark tile site in London (Podium) under sunlit conditions agreed well with the observation (Figure 13, left), whereas the values for shadowed sites and night-time radiant temperatures were underestimated, with a maximum difference between prediction and observation of 10 °C for the night-time. The simplification of setting the shadowed surface temperature equal to T_a results in an underestimation of $L\uparrow$. In addition, the T_{mrt} at the grass site (Garden, Figure 13, right) was underestimated. This could be because the properties of the grass and underlying soil at the site in London differed from those at the site used to gather the data used in the model's development, leading to the underestimation of $L\uparrow$. In addition, the modelled T_{mrt} at the grass site had a relatively large degree of scatter compared to the asphalt site. It was found that there were large differences between the forcing of $K\downarrow$ for a reference meteorological site and the actual value of $K\downarrow$ at the local site in some cases. This could be partly responsible for the large scatter.

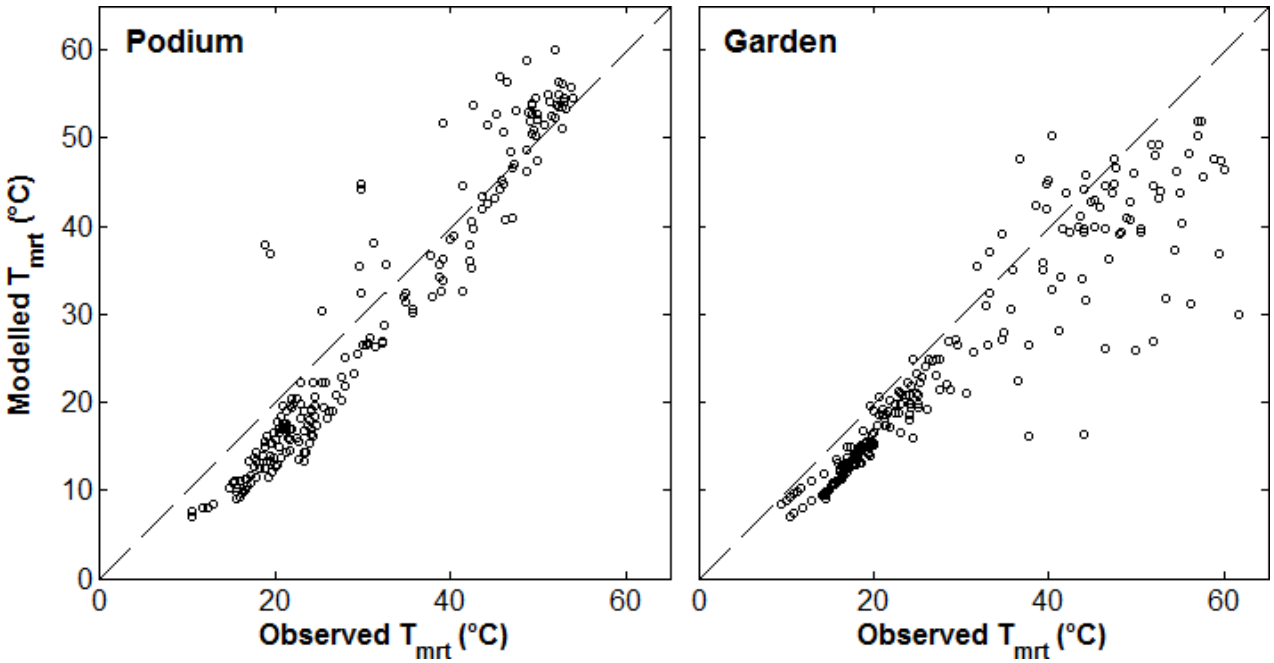

Figure 13. Scatterplot between observed and modelled values of the mean radiant temperature (T_{mrt}) at podium and garden site between the 7th and 16th of July, 2014 in London.

5. DISCUSSION

5.1. Modelling of urban site specific air temperature

The modelling of daytime and night-time T_a values (BLUEWS and NOCRAM, respectively) presented in **Papers I** and **II** performed reasonably well in terms of temporal development and accuracy (RMSE = 1.3 and 1.54 °C); their performance was comparable to that reported by Bohnenstengel et al. (2011) and Theeuwes et al. (2014), who coupled meso-scale models with a ULSM, and that reported by Erell and Williamson (2006) and Bueno et al. (2013) who developed analytical models.

The models developed in this work have several important advantages. First, they require only standard meteorological input data (e.g. $K\downarrow$, u and P) from a reference station and land surface information (e.g. land cover fractions, building heights and SVF values), which can be quickly calculated using geographic information system (GIS) data. Second, they can be executed using only general computational power (e.g. that offered by a personal computer). Third, the simplified modelling process makes it easy not just to run the models but to understand the underlying relationships between T_a and the influential factors such as building density and weather conditions.

These advantages allow users to simulate T_a at several places or cities as well as to test the effects of different parameters and model settings, for instance by altering the building density in a climate-sensitive urban planning exercise to see how this would affect T_a. Moreover, without appreciably increasing the computational load, the models can be combined with other models for predicting quantities such as building energy efficiency or human thermal comfort. As presented in Section 3, there is a plan to couple the models presented herein with the SOLWEIG model to provide urban site-specific T_a values for use in the computation of T_{mrt}.

There are however several aspects of the models that could be improved or refined. The CBL model in BLUEWS preferably uses initial values of θ, q and z_i and the vertical gradients of θ and q at the top of the CBL that must be obtained via observation, for instance by radiosonde measurements. Such data are not widely available, especially in urban areas. Because reliable initial values of z_i and vertical gradients of θ and q, are particularly difficult to obtain, sensitivity tests were conducted (Section 5.3 and Figure 11 in **Paper I)** to assess how these parameters affect the accuracy of the prediction of T_a with BLUEWS. The results support the use of typical values based on boundary layer measurements but suggest that the input values must lie within a certain range of the true value to achieve satisfactory performance. The extent to which the typical values used in this work can be applied in other contexts should therefore be tested by evaluating the model against data for other cities.

One way of refining BLUEWS would be to transfer the values of T_a predicted above the RSL by the CBL into the UCL (thus at street level) rather than perturbing a reference T_a to obtain an urban site-specific T_a. One way of performing such a transfer is to apply the Monin-Obukhov similarity theory (e.g. Bohnenstengel et al. 2011; Theeuwes et al. 2014). However, the theory assumes a steady and horizontally homogeneous atmosphere, which is unlikely to be a good assumption in urban areas. Theeuwes (2015) explored the modification of the theory for urban areas and managed to obtain better results than were achieved with the original theory. This modified theory was actually tested during a preliminary study conducted prior to the work presented in **Paper I** but it did not produce T_a values that agreed acceptably with observation. As stressed by Theeuwes (2015), this method is not suitable for spatially complex and heterogeneous areas and its applicability to urban areas is debatable.

NOCRAM consistently exhibited small systematic errors (mean bias error is about 0.06 K h^{-1}) for all cloud and wind conditions (indicated by *CRIF*) as well as for both open and built-up sites used for the model development. These errors can be related to the parameterizations of the impact of *SVF* on CR_{peak} depending on *CRIF*, the simplified estimation of t_{peak} (as the mean of t_1 and t_2), and the impact of wind disturbances. To carefully evaluate the parameterization of the *SVF* impact, a large quantity of data on cooling rates at sites representing a wide range of *SVF* values under different wind and cloud conditions would be needed. The parameterizations of t_{peak} and wind disturbances could be improved by taking account of temporal series of information on atmospheric stability. In **Paper II** and **Paper III**, the timing of t_{peak} was found to correspond approximately to the point at which Ri_b turns from negative to positive.

There are several other factors that are known to influence nocturnal cooling but were not considered in NOCRAM, including the heterogeneity of surface materials (Oke 1988; Oke et al. 1991), evapotranspiration from vegetation (Holmer et al. 2013; Konarska et al. 2015), the release of anthropogenic heat (e.g. Arnfield 2003; Fan and Sailor 2005; Offerle et al. 2006; Ryu and Baik 2012), air humidity (Holmer et al. 2013) and advection of cooler/warmer air from the surroundings (Eliasson and Holmer 1990; Haeger-Eugensson and Holmer 1999; Thorsson and Eliasson 2003). Oke (1981) and Konarska et al. (2015) suggest that *SVF* explains more than 80 % of the spatial variation of the UHI/IUHI intensity or cooling rates so the factors listed above presumably explain the small residual variation. A simple way to account for their influence is to parameterize their contributions to cooling rates as was done for cloud and wind conditions by introducing the impact factor *CRIF*. Specifically, this could be partly done with a ULSM, which could compute all of the component fluxes in the SEB in a way that accounts for the urban land surface characteristics.

Furthermore, NOCRAM should be tested for other cities, preferably at lower latitudes than Gothenburg with high solar irradiation, and with different climate classes and/or different site characteristics. Some of the model's setting were statistically or empirically

determined, and while the model performed well when tested against independent datasets from Gothenburg and one from London, it probably retains some regional dependencies.

5.2. Nocturnal cooling in the near-surface atmosphere and implications to the modelling

Nocturnal cooling was found to develop differently in two layers of the atmosphere but also exhibited two-phase behaviour at all heights. Height-dependent variations in cooling rates around sunset (Phase 1) and the convergence of cooling rates a few hours after sunset (Phase 2) in the lower layer (up to 60-70 m) were also reported by Schaller (1977) and Sun et al. (2003). The Phase 1 cooling is driven by both radiative and sensible heat flux divergence. Radiative flux divergence near the surface is most pronounced around sunset due to surface radiative cooling, and rapidly decreases through the night (Sun et al. 2003). The flux divergence also depends on height (Steeneveld et al. 2010). The development of an inversion layer is probably governed by strong radiative flux divergence (e.g. Garratt and Brost 1981; Ha and Mahrt 2003). The positive values on Ri_b in the lower layer in Phase 1 (Figure 11) are consistent with this hypothesis. On the other hand, other studies (André and Mahrt 1982; Estournel et al. 1986; Grant 1997) have reported the significant influence of turbulent heat flux divergence on cooling rates. Notably, Schaller (1977) showed that sensible heat flux divergence starts in the early afternoon. Acevedo and Fitzjarrald (2001) reported that small-scale turbulence cascaded from daytime large-scale turbulence causes local air mixing in the early evening, generating spatial differences in cooling rates. This matches the rapid decrease in wind speed in Phase 1 (Figure 4 in **Paper III**). The convergence of cooling rates in Phase 2 can probably be attributed to reduced height-dependent variations in radiative flux divergence and mechanical turbulence. Due to the rapid decrease in surface temperature from sunset (Sun et al. 2003), long-wave radiative flux exchanges between the air and the surface become small but the long-wave radiative divergence continues in the atmosphere, stretching the stable layer. Therefore, variations in the radiative flux divergence between heights become small. Small-scale turbulence generated over the sub-urban site can also homogenize differences in cooling rates. The presence of a surface mixing layer below the elevated inversion layer has been observed, particularly within heterogeneous urban areas (Spanton and Williams 1988; Barlow et al. 2011). The bottom of the inversion layer has been estimated to lie at a height of around 40-70 m in Gothenburg (Eliasson and Holmer 1990), which corresponds approximately to the depth of the lower layer.

In the upper layer, the cooling rates diverge in Phase 1 and the height-dependent variations persist in Phase 2. In contrast to the lower layer, the cooling in this layer is probably triggered by sensible heat flux divergence as the atmospheric stability is nearly neutral in Phase 1 (Figure 11). According to the diagram of Schaller (1977), the ratio of radiative cooling rates to actual cooling rates decreases rapidly with height below 50 m above the ground. On the other hand, the cooling in Phase 2 is governed by long-wave radiative divergence as Ri_b increases and wind speed ceases (Figure 4 in Paper **III**). The

persistent height-dependent differences in cooling rates indicate that long-wave radiative divergence decreases with increasing height.

Variations in cooling between different synoptic conditions and seasons, previously reported by Holmer et al. (2007) and Chow and Svoma (2011), were also found in this study. The characteristic cooling development discussed above is most pronounced in spring, followed by summer and autumn under anti-cyclonic conditions, whereas the pattern is less distinctive in winter under anti-cyclonic conditions and in all seasons under cyclonic and directional flow conditions. The same is true for the magnitude of the cooling rates. This implies that the patterns of nocturnal cooling development in the near-surface atmosphere can be classified on the basis of synoptic weather types and seasons. It is also supported by Figures 5 and 6 in **Paper III,** which show that these conditions are associated with local wind and cloud conditions, which strongly affect cooling rates (Runnalls and Oke 2000)

Some findings presented in **Paper III** support the underlying concepts of the NOCRAM model and can be used in its further development. As exemplified in Figure 8, synoptic weather changes during the night can adversely affect the performance of NOCRAM. However, LWT stayed the same during night with the relatively high frequency (27% of the total study days). Furthermore, the frequency of the persistent synoptic weather situations could be higher in other regions as the variability of synoptic weather conditions is relatively high in northern Europe. For those reasons, the model can be more applicable in other climate zones. The relatively high frequency of persistent weather types also supports the model's use of bulk cloud conditions across the night (i.e. the use of the *CI* variable).

The cooling profiles measured at three heights in the lower layer (Figure 10) are all similar aside from the height dependence observed during Phase 1. This implies that the cooling rates calculated at 2 m using NOCRAM can be modified to predict cooling at other heights in this layer. Specifically, CR_{peak} in Phase 1 can be calculated as a function of the height, *CRIF*, T_{max} and *SVF*. In addition, it may be necessary to modify the parameterization of wind disturbance accounting for height-dependent variations in atmospheric stability.

5.3. Modelling of mean radiant temperature

When using the ground cover scheme developed in **Paper IV**, SOLWEIG simulates T_{mrt} reasonably well over different types of ground surfaces in sunlit locations. The asphalt surface increased T_{mrt} (+1.5 ˚C) relative to the reference cobbled surface whereas grass surfaces exhibited a lower T_{mrt} (- 5.2 ˚C).

However, the impact of different ground cover types is much smaller than the effect of shadowing (-38.2 °C). This suggests that altering ground surface materials may not be an

effective way of reducing radiant loads during heat wave episodes. In fact, the effect of altering surface materials on the thermal environment is not straightforward. Increasing the albedo of surfaces reduces long wave radiation fluxes, but is counterbalanced by increased reflection of shortwave radiation (Erell et al. 2014). Surface temperatures on moist grass are reduced by latent heat, but the surface's thermal admittance increased by higher soil moisture content reduces the rate of heat release (Oke 1987). However, modifying surface materials may be a viable way of partially reducing T_{mrt} in areas where shadowing is not an option.

The evaluation of the ground cover scheme showed that while T_{mrt} at the dark tile site was successfully modelled, T_{mrt} at the grass site was underestimated and deviated more strongly from the observations than was the case for the dark tile site. It appears that T_{mrt} can vary with the maintenance of grass and the type of grass and soil. The characteristics of grass surfaces vary more dynamically than those of asphalt due to changes in the soil moisture content and the growth of grass. This also gives rise to difficulties in estimating latent heat fluxes and storage heat fluxes for grass surfaces in ULSMs (Grimmond et al. 2010). In addition, the shadowed and night-time T_{mrt} was underestimated as those values are set to be T_a. A parameterization for predicting T_s values will be improved either with the acquisition of more reference data at various sites or with the much more complex surface temperature scheme. However, the latter method increases computational load dramatically. The advantage of the simple ground cover scheme in SOLWEIG makes it possible to examine micro-scale radiation fluxes for relatively extensive areas.

The modelled T_{mrt} is most sensitive to $K\downarrow$, followed by T_a (**Paper I** and **IV**). Large discrepancies between the forcing of $K\downarrow$ at the reference site and the actual value over the site for which the simulation is performed were observed and consequently led to the poor modelling of T_{mrt}. Cloudiness can differ between the sites if they are far from each other, especially on semi-cloudy days. Particularly when high time resolution is used for the simulation, this can significantly influence the model output. As seen in Figure 7, T_a differs between sites depending on the surface characteristics. The use of non-site specific T_a in the modelling of T_{mrt} can cause systematic errors. T_a used should be representative of the urban area where T_{mrt} is calculated. The modelling of T_a with BLUEWS and NOCRAM could potentially improve the prediction of T_{mrt}.

5.4. Potential usage of the developed models

The models developed in this thesis can be used for applications other than estimating human thermal comfort. For example, urban site specific T_a values can be used to model micro-scale surface energy balance. Thus the models can be used for the estimation of building energy efficiency and thermal conditions (e.g. frost) on road surfaces. Cooling rates have been used to estimate the depth of an air layer involved in nocturnal cooling (Holmer et al. 2012). This depth could correspond to the depth of a stable boundary layer, which is useful of the calculation of air pollutant concentration.

6. CONCLUSIONS

The main results and conclusions are summarized as follows:

- Day-time and night-time models (BLUEWS and NOCRAM) for computing urban site specific air temperatures have been developed. BLUEWS was developed by coupling a convective boundary layer slab model and an urban land surface model. NOCRAM was empirically developed based on the concept of nocturnal cooling progressing in two distinct phases. The models were designed to require only standard meteorological input data together with information on the land surface, and can be run using general computational resources, all of which are widely available. The daytime and night-time models show reasonably good performance in terms of temporal development and accuracy (RMSE = 1.3 and 1.54 ˚C, respectively).

- Analysis of nocturnal cooling in the near-surface atmosphere (up to 105 m above the ground) at a suburban site in Gothenburg shows that nocturnal cooling develops differently in two layers. The more intense cooling occurs in the lower layer, which extends from the ground surface to a height of 60-70 m. In both layers, there was a two-phase division of cooling. Around sunset, the cooling rates diverge decreasing with increasing height in the two layers. However, within a few hours after sunset, cooling rates in the lower layer converge, while the height-dependent cooling rate differences in the upper layer remain largely unchanged over the rest of the night. The persistent height-dependent differences in the upper layer are linked to the formation of a stabilized atmospheric layer. The trends and the cooling intensity vary with the synoptic weather situations and seasons. Those are most pronounced in spring and summer under anti-cyclonic conditions. The results in this analysis imply that NOCRAM could be applied to other heights with a few modifications.

- A ground cover scheme in the SOLWEIG model was developed based on field observations in Gothenburg to calculate mean radiant temperatures over different ground cover types in a sunlit location. The mean radiant temperatures for three ground cover materials (grass, asphalt and cobble stone) differed by only a few degrees, or approximately one tenth of the difference between sunlit and shadowed areas. This suggests that modifying ground cover types would be less effective than increasing shadowing as a way of reducing daytime radiant heat load. Evaluations of the model revealed that T_{mrt} was modelled reasonably well over different ground cover types in London, UK.

7. FUTURE OUTLOOK

- BLUEWS, NOCRAM and SOLWEIG will be implemented into a climate service tool called UMEP. To increase the models' availability, it will be important to keep updating their constituent sub-models to improve their estimations, and to test them against data for different areas and cities from several climate zones.

- While the relationship between cooling rates and *SVF* has been extensively studied, there are fewer studies on the quantitative impact of other influential factors (surface materials, vegetation and anthropogenic heat) on cooling rates. It will be important to clarify the effects of these factors in order to identify reliable methods for reducing urban heat loads.

- The physical processes involved in near-surface nocturnal cooling and the evolution of the night-time boundary layer are not fully understood yet, especially within urban areas. Despite the unsteady state of the night-time atmosphere, there is a lack of long-term observational data covering periods including different weather conditions and seasons. The acquisition of long-term datasets of air temperature, turbulence and radiation with fine spatial resolutions in the near-surface atmosphere could thus greatly increase our understanding of these phenomena.

ACKNOWLEDGEMENTS

I would like to acknowledge my supervisors, colleagues, friends and family, who have supported this PhD project and me during this study.

First, I would like to thank my supervisors for all the supports during this study. To Prof. Sofia Thorsson, for trying to understand my situation, seeking better solutions and encouraging me with various ways. To Dr. Fredrik Lindberg, for supporting all the details in my study and connecting me to many international researchers and to Prof. Björn Holmer for uncountable and fruitful discussions, continuous supports and stimulating my curiosity for research. To Dr. David Rayner, for useful advice and comments on my papers.

I would also like to thank my examiner, Prof. Deilang Chen for his valuable advice and generous attitude to my study, and acknowledge Prof. Sue Grimmond from the University of Reading, UK, for involving me in the modelling world of the urban atmosphere and supporting my study with her great knowledge and management.

I am grateful to my colleagues in King's College and University of Reading, UK. My research has been supported by Dr. Simone Kotthaus, Mr. William Morrison and Mr. John Mustchin who have carefully maintained field measurements in London and data quality. I would like to thank Dr. Helen Ward as well as Dr. Leena Järvi from University of Helsinki for supporting the model development.

I would like to thank my colleagues at GVC. Especially to Yumei Hu for sharing experiences, various discussions and fikas. To Tinghai Ou, Andrea Seim, Andreas Johnsson, Hongxing He and Selma Pacariz for having random chats but also giving me many pieces of advice. To my office roommates, Frans Olofson, Esben Almkvist and Ardo Robijn for creating nice work environments and various chats, and sometimes helping me solve some troubles. Many thanks to my past roommate and friend, Irina Polovodova Asteman, for encouragement, company for swimming and weekend fikas, and sharing your family time. A special thanks to Janina Konarska for her company at various places, supports on my study and inspiring my research motivation. Janka, I am also very happy that we could study together. I will remember our study life with many funny accidents we have experienced during the past five years. All other colleagues are also acknowledged.

I would like to acknowledge Prof. Tsuyoshi Honjo from Chiba University for giving advice on my study, listening to my worries and bring some Japanese products which I miss in Sweden, and also thank Dr. Kevin Lau from the Chinese University of Hong Kong for keeping the update of his research and bring up some ideas for my study.

I am also grateful to Prof. Manabu Kanda from my former university, for showing me how exciting urban climate and meteorology are when I was a bachelor and master. This

journey is definitely originated at that time. Also thanks to Kanda's lab members for keeping encouraging and inspiring me by their own research.

I would like to thank my friends in Gothenburg, Japan and many other places. Especially to Yutaka Goto for useful comments on my study and great encouragement to my both academic and private life. To Jun Kono and Kazutoshi Sagi, for sharing experiences during university life and making me laugh often. To Yuki Tashiro, Mariya Kato, Chiaki Horita, Satoko Takahashi, for showing me the shining world of music and dance, and giving a special break. I was so lucky I could meet you all in Gothenburg. In addition, I would like to thank my Karate instructors and fellows for the enjoyable time.

Finally, I would like to thank my family so much, for all the supports, caring about my situation and believing in me. Especially, without my parents' support, I would not have reached here. Many thanks for encouraging me anytime when I need, even with the long distance and long time lag between Japan and Sweden. 本当にありがとう。

This study was financially supported by:

- The Swedish Research Council FORMAS,
- The Swedish Energy Agency,
- The Swedish Environmental Protection Agency,
- The Swedish National Heritage Board,
- The Swedish Transport Administration,
- The Swedish Society for Anthropology and Geography,
- EmBRACE,
- Paul and Marie Berghaus Donation Scholarship,
- Professor Sven Lindqvist Research Foundation.

REFERENCES

Acevedo, O., and D. Fitzjarrald, 2003: In the core of the night-effects of intermittent mixing on a horizontally heterogeneous surface. *Bound.-Layer Meteor.*, **106,** 1-33.

Acevedo, O. C., and D. R. Fitzjarrald, 2001: The early evening surface-layer transition: temporal and spatial variability. *J. Atmos. Sci.*, **58,** 2650-2667.

Andersson-Sköld, Y., S. Thorsson, D. Rayner, F. Lindberg, S. Janhäll, A. Jonsson, U. Moback, R. Bergman, and M. Granberg, 2015: An integrated method for assessing climate-related risks and adaptation alternatives in urban areas. *Clim. Risk Manage.*, **7,** 31-50.

André, J. C., and L. Mahrt, 1982: The nocturnal surface inversion and influence of clear-air radiative cooling. *J. Atmos. Sci.*, **39,** 864-878.

Arnfield, A. J., 2003: Two decades of urban climate research: a review of turbulence, exchanges of energy and water, and the urban heat island. *Int. J. Climatol.*, **23,** 1-26.

Ashie, Y., T. Kono, and K. Takahashi, 2005: Development of numerical simulation model of urban heat island, Annual report of the earth simulator center, 85–88 pp.

ASHRAE, 2001: *Fundamentals Handbook*. American Society of Heating, Refrigerating, and Air-Conditioning Engineers, Atlanta.

Baklanov, A., S. Grimmond, A. Mahura, and M. Athanassiadou, 2009: *Meteorological and Air Quality Models for Urban Areas*. Springer, Berlin, Heidelberg.

Barlow, J. F., 2014: Progress in observing and modelling the urban boundary layer. *Urban Climate*, **10, Part 2,** 216-240.

Barlow, J. F., T. M. Dunbar, E. G. Nemitz, C. R. Wood, M. W. Gallagher, F. Davies, E. O'Connor, and R. M. Harrison, 2011: Boundary layer dynamics over London, UK, as observed using Doppler lidar during REPARTEE-II. *Atmos. Chem. Phys.*, **11,** 2111-2125.

Bogren, J., T. Gustavsson, M. Karlsson, and U. Postgård, 2000: The impact of screening on road surface temperature. *Meterol. Appl.*, **7,** 97-104.

Bohnenstengel, S. I., S. Evans, P. A. Clark, and S. E. Belcher, 2011: Simulations of the London urban heat island. *Quar. J. R. Meteor. Soc.*, **137,** 1625-1640.

Bueno, B., L. Norford, J. Hidalgo, and G. Pigeon, 2013: The urban weather generator. *J. Bldg. Perf. Sim.*, **6,** 269-281.

Chen, D., 2000: A monthly circulation climatology for Sweden and its application to a winter temperature case study. *Int. J. Climatol.*, **20,** 1067-1076.

Chen, Y.-C., T.-P. Lin, and A. Matzarakis, 2014: Comparison of mean radiant temperature from field experiment and modelling: a case study in Freiburg, Germany. *Theor. Appl. Climatol.*, **118,** 535-551.

Chow, W. T. L., and M. Roth, 2006: Temporal dynamics of the urban heat island of Singapore. *Int. J. Climatol.*, **26,** 2243-2260.

Chow, W. T. L., and B. M. Svoma, 2011: Analyses of nocturnal temperature cooling-rate response to historical local-scale urban land-use/land cover change. *J. Appl. Meteor. Climatol.*, **50,** 1872-1883.

Cleugh, H. A., and C. S. B. Grimmond, 2001: Modelling regional scale surface energy exchanges and cbl growth in a heterogeneous, urban-rural landscape. *Bound.-Layer Meteor.*, **98,** 1-31.

Crawford, T. M., and C. E. Duchon, 1999: An improved parameterization for estimating effective atmospheric emissivity for use in calculating daytime downwelling longwave radiation. *J. Appl. Meteor.*, **38,** 474-480.

de Bruin, H. A. R., and A. A. M. Holtslag, 1982: A simple parameterization of the surface fluxes of sensible and latent-heat during daytime compared with the penman-monteith concept. *J. Appl. Meteor.*, **21,** 1610-1621.

Eliasson, I., and B. Holmer, 1990: Urban heat island circulation in Göteborg, Sweden. *Theor. Appl. Climatol.*, **42,** 187-196.

Erell, E., and T. Williamson, 2006: Simulating air temperature in an urban street canyon in all weather conditions using measured data at a reference meteorological station. *Int. J. Climatol.*, **26,** 1671-1694.

Erell, E., D. Pearlmutter, D. Boneh, and P. B. Kutiel, 2014: Effect of high-albedo materials on pedestrian heat stress in urban street canyons. *Urban Climate*, **10, Part 2,** 367-386.

Estournel, C., R. Vehil, and D. Guedalia, 1986: An observational study of radiative and turbulent cooling in the nocturnal boundary layer (ECLATS experiment). *Bound.-Layer Meteor.*, **34,** 55-62.

Fan, H., and D. J. Sailor, 2005: Modeling the impacts of anthropogenic heating on the urban climate of Philadelphia: a comparison of implementations in two PBL schemes. *Atmos. Environ.*, **39,** 73-84.

Fortuniak, K., K. Kłysik, and J. Wibig, 2006: Urban–rural contrasts of meteorological parameters in Łódź. *Theor. Appl. Climatol.*, **84,** 91-101.

Galarneau, T. J., T. M. Hamill, R. M. Dole, and J. Perlwitz, 2012: A multiscale analysis of the extreme weather events over western Russia and northern Pakistan during July 2010. *Mon. Weather Rev.*, **140,** 1639-1664.

Garratt, J. R., 1992: *The atmospheric boudanry layer*. Cambridge University Press, Cambridge.

Garratt, J. R., and R. A. Brost, 1981: Radiative cooling effects within and above the nocturnal boundary layer. *J. Atmos. Sci.*, **38,** 2730-2746.

Grant, A. L. M., 1997: An observational study of the evening transition boundary-layer. *Quar. J. R. Meteor. Soc.*, **123,** 657-677.

Grimmond, C. S. B., and T. R. Oke, 1995: Comparison of heat fluxes from summertime observations in the suburbs of four north American cities. *J. Appl. Meteor.*, **34,** 873-889.

Grimmond, C. S. B., and T. R. Oke, 2002: Turbulent heat fluxes in urban areas: Observations and a local-scale urban meteorological parameterization scheme (LUMPS). *J. Appl. Meteor.*, **41,** 792-810.

Grimmond, C. S. B., T. R. Oke, and H. A. Cleugh, 1993: The role of rural in comparisons of observed suburban-rural flux differences. *Exchange processes at the land surface for a range of space and time scales*, Yokohama, *International Association of Hydrological Sciences Publication*, **212**, 165-174.

Grimmond, C. S. B., M. Blackett, M. J. Best, J. Barlow, J. J. Baik, S. E. Belcher, S. I. Bohnenstengel, I. Calmet, F. Chen, A. Dandou, K. Fortuniak, M. L. Gouvea, R. Hamdi, M. Hendry, T. Kawai, Y. Kawamoto, H. Kondo, E. S. Krayenhoff, S. H. Lee, T. Loridan, A. Martilli, V. Masson, S. Miao, K. Oleson, G. Pigeon, A. Porson, Y. H. Ryu, F. Salamanca, L. Shashua-Bar, G. J. Steeneveld, M. Tombrou, J. Voogt, D. Young, and N. Zhang, 2010: The international urban energy balance models comparison project: first results from Phase 1. *J. Appl. Meteor. Climatol.*, **49,** 1268-1292.

Ha, K.-J., and L. Mahrt, 2003: Radiative and turbulent fluxes in the nocturnal boundary layer. *Tellus A*, **55,** 317-327.

Haeger-Eugensson, M., and B. Holmer, 1999: Advection caused by the urban heat island circulation as a regulating factor on the nocturnal urban heat island. *Int. J. Climatol.*, **19,** 975-988.

Holmer, B., S. Thorsson, and I. Eliasson, 2007: Cooling rates, sky view factors and the development of intra-urban air temperature differences. *Geografiska Annaler Series a-Phys. Geogr*, **89A,** 237-248.

Holmer, B., S. Thorsson, and J. Lindén, 2013: Evening evapotranspirative cooling in relation to vegetation and urban geometry in the city of Ouagadougou, Burkina Faso. *Int. J. Climatol.*, **33,** 3089-3105.

Holmer, B., S. Thorsson, J. Lindén, and C. S. B. Grimmond, 2012: Urban nocturnal cooling – a two-phase development. *ICUC8 – 8th International Conference on Urban Climates,*, UCD, Dublin Ireland.

Johnson, D. B., 1985: Urban modification of diurnal temperature cycles in birmingham, U.K. *Int. J. Climatol.*, **5,** 221-225.

Järvi, L., C. S. B. Grimmond, and A. Christen, 2011: The Surface Urban Energy and Water balance Scheme (SUEWS): Evaluation in Los Angeles and Vancouver. *J. Hydrol.*, **411,** 219-237.

Kanda, M., 2006: Atmospheric boundary layer and scalar dispersion with explicitly resolved urban geometries using Large eddy simulation for city. *Sixth Symposium on the Urban Environment, American Meteorological Society*, Atlanta, GA.

Kidder, S. Q., and O. M. Essenwanger, 1995: The effect of clouds and wind on the difference in nocturnal cooling rates between urban and rural areas. *J. Appl. Meteor.*, **34,** 2440-2448.

Konarska, J., B. Homer, F. Lindberg, and S. Thorsson, 2015: Influence of vegetation and building geometry on the spatial variations of air temperature and cooling rates in a high latitude city. *Int. J. Climatol.* doi: dx.doi.org/10.1002/joc.4502

Lamb, H. H., 1950: Types and spells of weather around the year in the British Isles : Annual trends, seasonal structure of the year, singularities. *Quar. J. R. Meteor. Soc.*, **76,** 393-429.

Lau, K. K.-L., C. Ren, J. Ho, and E. Ng, 2015: Numerical modelling of mean radiant temperature in high-density sub-tropical urban environment. *Energy Build.*, **114,** 80–86.

Lee, D. O., 1979: Contrasts in warming and cooling rates at an urban and a rural site. *Weather*, **34,** 60-66.

Lindberg, F., and C. S. B. Grimmond, 2010: Continuous sky view factor maps from high resolution urban digital elevation models. *Climate Res.*, **42,** 177-183.

Lindberg, F., and C. S. B. Grimmond, 2011: The influence of vegetation and building morphology on shadow patterns and mean radiant temperatures in urban areas: model development and evaluation. *Theor. Appl. Climatol.*, **105,** 311-323.

Lindberg, F., B. Holmer, and S. Thorsson, 2008: SOLWEIG 1.0 - Modelling spatial variations of 3D radiant fluxes and mean radiant temperature in complex urban settings. *Int. J. Biometeorol.*, **52,** 697-713.

Lindberg, F., C. S. B. Grimmond, S. Onomura, and L. Järvi, 2015: UMEP - An integrated tool for urban climatology and climate sensitive planning applications. *9th International Conference on Urban Climate jointly with 12th Symposium on the Urban Environment*, Toulouse, France.

Loridan, T., C. S. B. Grimmond, B. D. Offerle, D. T. Young, T. E. L. Smith, L. Järvi, and F. Lindberg, 2010: Local-scale Urban Meteorological Parameterization Scheme (LUMPS): Longwave radiation parameterization and seasonality-related developments. *J. Appl. Meteor. Climatol.*, **50,** 185-202.

Magee, N., J. Curtis, and G. Wendler, 1999: The urban heat island effect at Fairbanks, Alaska. *Theor. Appl. Climatol.*, **64,** 39-47.

Mayer, H., and P. Höppe, 1987: Thermal comfort of man in different urban environments. *Theor. Appl. Climatol.*, **38,** 43-49.

Offerle, B., C. S. B. Grimmond, K. Fortuniak, K. Kłysik, and T. R. Oke, 2006: Temporal variations in heat fluxes over a central European city centre. *Theor. Appl. Climatol.*, **84,** 103-115.

Oke, T., 1981: Canyon geometry and the nocturnal urban heat island: comparison of scale model and field observations. *J. Climatol*, **1,** 237-254.

Oke, T., G. Johnson, D. Steyn, and I. Watson, 1991: Simulation of surface urban heat islands under 'ideal'conditions at night part 2: Diagnosis of causation. *Bound.-Layer Meteor.*, **56,** 339-358.

Oke, T. R., 1976: The distinction between canopy and boundary layer urban heat islands. *Atmosphere*, **14,** 268-277.

Oke, T. R., 1987: *Boundary layer climates*. 2nd ed. Routledge, London and New York.

Oke, T. R., 1988: The urban energy-balance. *Prog. Phys. Geograp.*, **12,** 471-508.

Oke, T. R., and G. B. Maxwell, 1975: Urban heat island dynamics in Montreal and Vancouver. *Atmos. Environ.*, **9,** 191-200.

Pfahl, S., 2014: Characterising the relationship between weather extremes in Europe and synoptic circulation features. *Nat. Hazards Earth Syst. Sci.*, **14,** 1461-1475.

Raupach, M. R., 2001: Combination theory and equilibrium evaporation. *Quar. J. R. Meteor. Soc.*, **127,** 1149-1181.

Runnalls, K. E., and T. R. Oke, 2000: Dynamics and controls of the near-surface heat island of Vancouver, British Columbia. *Phys. Geogr,* **21,** 283-304.

Ryu, Y.-H., and J.-J. Baik, 2012: Quantitative analysis of factors contributing to urban heat island intensity. *J. Appl. Meteor. Climatol.*, **51,** 842-854.

Schaller, E., 1977: Time and height variability of the sensible heat flux in the surface layer. *Bound.-Layer Meteor.*, **11,** 329-354.

Spanton, A. M., and M. L. Williams, 1988: A comparison of the structure of the atmospheric boundary layers in Central London and a rural/suburban site using acoustic sounding. *Atmos. Environ.*, **22,** 211-223.

Steeneveld, G.-J., 2014: Current challenges in understanding and forecasting stable boundary layers over land and ice. *Front. Environ. Sci.*, **2,** 1-6.

Steeneveld, G. J., M. J. J. Wokke, C. D. Groot Zwaaftink, S. Pijlman, B. G. Heusinkveld, A. F. G. Jacobs, and A. A. M. Holtslag, 2010: Observations of the radiation divergence in the surface layer and its implication for its parameterization in numerical weather prediction models. *J. Geophys. Res. Atmos.*, **115,** 1-13.

Stewart, I. D., T. R. Oke, and E. S. Krayenhoff, 2013: Evaluation of the 'local climate zone' scheme using temperature observations and model simulations. *Int. J. Climatol.*, **34,** 1062–1080.

Stull, R. B., 1988: *An introduction to boundary layer meteorology* Kluwer Academic Publishers, Dordrecht.

Sun, J., S. P. Burns, A. C. Delany, S. P. Oncley, T. W. Horst, and D. H. Lenschow, 2003: Heat balance in the nocturnal boundary layer during CASES-99. *J. Appl. Meteor.*, **42,** 1649-1666.

Tennekes, H., and A. G. M. Driedonks, 1981: Basic entrainment equations for the atmospheric boundary layer. *Bound.-Layer Meteor.*, **20,** 515-531.

Theeuwes, N. E., 2015: Urban heat - natural and anthropogenic factors influencing urban air temperatures, Socio-economic and natural sciences of the environment, Wageningen University, 160 pp.

Theeuwes, N. E., G. J. Steeneveld, R. J. Ronda, B. G. Heusinkveld, L. W. A. van Hove, and A. A. M. Holtslag, 2014: Seasonal dependence of the urban heat island on the street canyon aspect ratio. *Q. J. R. Meteorolog. Soc.*, **140,** 2197–2210.

Thorsson, S., and I. Eliasson, 2003: An intra-urban thermal breeze in Göteborg, Sweden. *Theor. Appl. Climatol.*, **75,** 93-104.

Thorsson, S., F. Lindberg, I. Eliasson, and B. Holmer, 2007: Different methods for estimating the mean radiant temperature in an outdoor urban setting. *Int. J. Climatol.*, **27,** 1983-1993.

Thorsson, S., J. Rocklöv, J. Konarska, F. Lindberg, B. Holmer, B. Dousset, and D. Rayner, 2014: Mean radiant temperature – A predictor of heat related mortality. *Urban Climate*, **10,** 332-345.

United Nations, D. o. E. a. S. A., Population Division 2014: World Urbanization Prospects: The 2014 Revision, Highlights (ST/ESA/SER.A/352).

Upmanis, H., I. Eliasson, and S. Lindqvist, 1998: The influence of green areas on nocturnal temperatures in a high latitude city (Göteborg, Sweden). *Int. J. Climatol.*, **18,** 681-700.